GE Hitachi Nuclear Energy

James C. Kinsey
Vice President, ESBWR Licensing

PO Box 780 M/C A-55
Wilmington, NC 28402-0780
USA

T 910 675 5057
F 910 362 5057
jim.kinsey@ge.com

Security Notice
This letter forwards Security-Related information in accordance with 10CFR2.390. Upon removal of Enclosure 2 the balance of this letter may be considered non-Security-related.

MFN 08-380

Docket No. 52-010

May 6, 2008

U.S. Nuclear Regulatory Commission
Document Control Desk
Washington, D.C. 20555-0001

Subject: **Response to Portion of NRC Request for Additional Information Letters No. 121 and 132 Related to ESBWR Design Certification Application, RAI Number 19.2-41 S02 and 19.2-86 Respectively**

The purpose of this letter is to submit the GE Hitachi Nuclear Energy (GEH) response to the U.S. Nuclear Regulatory Commission (NRC) Request for Additional Information (RAI) sent by NRC letters dated December 5, 2007 (Reference 1) and January 15, 2008 (Reference 2). Previous RAIs were transmitted in References 3 as well as provided at the February 5, 2007 NRC Fragility Audit. RAI responses were provided in References 4 and 5. The GEH responses to RAI Numbers 19.2-41 S02 and 19.2-86 are in Enclosure 1.

Enclosure 2 contains Security-Related information identified by the designation "**{{{Security-Related Information - Withhold Under 10 CFR 2.390}}}**." GEH hereby requests this information be withheld from public disclosure in accordance with the provisions of 10 CFR 2.390. The public version is contained in Enclosure 3.

Verified DCD changes associated with this RAI response are identified in the enclosed DCD markups by enclosing the text within a black box. The marked-up pages may contain unverified changes in addition to the verified changes resulting from this RAI response. Other changes shown in the markup(s) may not be fully developed and approved for inclusion in DCD Revision 5.

D068
NRO

If you have any questions or require additional information, please contact me.

Sincerely,

James C. Kinsey

James C. Kinsey
Vice President, ESBWR Licensing

References:

1. MFN-07-658. Letter from U.S. Nuclear Regulatory Commission to Robert E. Brown, *Request For Additional Information Letter No. 121 Related To ESBWR Design Certification Application,* December 5, 2007

2. MFN 08-040, Letter from U.S. Nuclear Regulatory Commission to Robert E. Brown, *Request For Additional Information Letter No. 132 Related To ESBWR Design Certification Application*, dated January 15, 2008

3. MFN 06-237, Letter from U.S. Nuclear Regulatory Commission to David Hinds, *Request for Additional Information Letter No. 43 Related to ESBWR Design Certification Application*, July 18, 2006

4. MFN 06-268, Response to Portion of NRC Request for Additional Information Letter No. 43 Related to ESBWR Design Certification Application – ESBWR Containment Design and Probabilistic Risk Assessment Re: Containment Fragility Analysis – (Release A) RAI Numbers 6.2-95,6.2-97, 19.2-41, 19.2-44 to 19.2-46, 19.2-49, 19.2-50 and 19.2-57, August 12, 2006

5. MFN 06-268, Supplement 1 Supplemental Response to Portion of NRC Request for Additional Information Letter No. 43 Related to ESBWR Design Certification Application - Supplement 1 RAI Numbers 6.2-95 S1, 6.2-97 S1. 19.2-41 S1, 19.2-44 S1, 19.2-45 S1, 19.2-46 S1, 19.2-49 S1, 19.2-50 S1 and 19.2-57 S1, April 13, 2007

Enclosures:

1. Response to Portion of NRC Request for Additional Information Letters No. 121 and 132 Related to ESBWR Design Certification Application, ESBWR Probabilistic Risk Assessment, RAI Numbers 19.2-41 S02 and 19.2-86 Respectively

2. Figures 3G.1-52 and 3G.1-53 *Security-Related*

3. Figures 3G.1-52 and 3G.1-53 *Non Security-Related*

cc: AE Cubbage USNRC (with enclosure)
GB Stramback GEH/San Jose (with enclosure)
RE Brown GEH/Wilmington (with enclosure)
DH Hinds GEH/Wilmington (with enclosure)
eDRF Section 0000-0078-7338

Enclosure 1

MFN 08-380

Response to Portion of NRC Request for Additional Information Letters No. 121 and 132 Related to ESBWR Design Certification Application ESBWR Probabilistic Risk Assessment RAI Numbers 19.2-41 S02 and 19.2-86 Respectively

*Verified DCD changes associated with this RAI response are identified in the enclosed DCD markups by enclosing the text within a black box. The marked-up pages may contain unverified changes in addition to the verified changes resulting from this RAI response. Other changes shown in the markup(s) may not be fully developed and approved for inclusion in DCD Revision 5.

NRC RAI 19.2-41

In DCD Tier 2, 19.2.4, GE only provides a reference to the GE Probabilistic Risk Assessment (PRA) report. The detailed fragility analysis for containment ultimate strength is contained in the GE PRA report, Revision 1, Appendix B.8. It is unclear how the 10 CFR Part 50.44(c)(5) requirement is addressed. It is also unclear how the SECY 93-087 requirement, which requires satisfaction of Service Level C limits, including considerations of structural instability, for the more likely severe accident challenges for approximately 24 hours following the onset of core damage under most likely severe accident challenges, and, following this period the containment should continue to provide a barrier against the uncontrolled release of fission products, is satisfied by the fragility analysis. Provide the following information in ESBWR DCD Tier 2, Section 19.2.4:

a) A summary of the GE PRA report, Revision 1, Appendix B.8, including all pertinent results;

b) A discussion of how the 10 CFR Part 50.44(c)(5) requirement and the SECY 93-087 requirement are satisfied;

c) Available test data of over-pressurization of containment structures similar to the ESWR design (with more geometric discontinuities than typical containments in the current fleet of reactors) at both ambient and severe temperature environments.

GE Response

a) The GE PRA report, Revision 1, Appendix B.8 will be moved to the DCD Chapter 19 the next DCD revision.

b) The 10 CFR Part 50.44(c)(5) requirement and the SECY 93-087 requirement are satisfied by meeting the ASME Section III acceptance criteria of Service Level C or Factored Load Category stipulated in RG 1.7 Revision 3. Details are documented in DCD Section 6.2.5.4.2.

c) Available test data of over-pressurization of containment structures relevant to ESBWR reinforced concrete containment vessel (RCCV) are two tests conducted by Sandia National Laboratories: a reinforced containment 1/6th scale test conducted in the late eighties and the more recent ¼ scale test of a pre-stressed containment. However, in order to appropriately interpret the results of these two tests relative to ESBWR, we must know the limitations on our abilities to simulate experimentally the failure behavior of concrete containments.

Concrete containment failure mode under internal pressure is critically dependent on the pressurization medium, gas or water. The most likely failure mode for concrete containments, whether reinforced or pre-stressed, tested under water pressurization is burst, while gas pressurization would produce only leakage. This has to do with the balance between the rate of pressurization and the rate of depressurization at the instant of failure initiation by liner cracking or other venting mechanisms. Under water

pressurization, a tiny change in the volume of the nearly incompressible fluid requires a huge pressure increment, whereas for gas pressurization the opposite is true. This implies that the pumping rate of the pressurization medium at the instant of failure initiation governs the failure mode. Behavioral differences between the reinforced and pre-stressed structures, namely, ductile behavior for the former and brittle behavior for the latter, can alter the failure mode if the pressurization medium is changed. For example, a pre-stressed containment could fail in a ductile manner, i.e. in a leak-before-break mode, under gas pressure. Therefore, one should be careful in using the test results directly to predict containment behavior under over-pressurization.

The experimental evidence shows that the failure mode for reinforced concrete containments internally pressurized by gas (air or nitrogen) is by leakage through liner cracks at points of discontinuity such as at stud locations, insert plates or thickened flanges around penetration covers. The Sandia 6th Scale reinforced concrete model confirmed this behavior. The leakage pressure for that test was 145 psig, which is 3.22 times design pressure. At 145 psig, the model could not be pressurized further, and for reasons mentioned above the pressurization rate could not keep up with the leakage rate. On the other hand, Sandia's 1/4th scale model of a pre-stressed concrete containment failed catastrophically at 3.6 times the design pressure. In this case, the rupture of the hoop tendons caused very sudden loss of structural stiffness, which overwhelmed the ability of the liner to form fuse-like pressure relief mechanism. The question is: if the pressurization medium were air instead of water, would the failure have been a catastrophic burst? Most likely it would be a leakage type failure, despite the brittle nature of the structure, but of a different, perhaps somewhat larger, configuration than in reinforced concrete. It should be noted parenthetically that the 3.6-factor was predicted using simple hand calculations. The leak-before-break failure mode could not be demonstrated in large-scale models because of the very large air volume required.

The robust design of the concrete pressure boundary of ESBWR is expected to perform significantly better than the Sandia 1/6th scale model, even considering its geometric discontinuities. However, treating the 1/6th scale model as a guide for judging the ultimate pressure capacity of ESBWR's concrete pressure boundary, we can use the global strain as an indicator. An axi-symmetric global analysis of the Sandia model, and the measured far field liner strains, gave a value of about 1.1% at ultimate pressure for a mid-height location, about the same elevation as the failure location in the insert plate (see Figure 5.3.6 in NUREG/CR 5341, SAND89-0349, dated October 1989). Clearly, the failure strain in the insert plate must have been several times this value due to strain concentration at the discontinuity. If we were to assume that a similar far field strain value would cause failure in the ESBWR liner at a point of discontinuity, we would conclude that for the ESBWR to develop failure in its concrete pressure boundary, the global analysis must show a far field strain value of at least 1%. As shown in Table B.8-1 of the PRA report, the maximum liner strain calculated by ANSYS nonlinear analysis is only 0.165% which is well within the code allowable when the internal pressure is as high as 1.468 MPa (4.7 times design pressure). Such a large margin should easily compensate for the lack of data at high temperature.

The above discussion indicates that the ESBWR containment ultimate pressure capacity would not be controlled by the concrete strength. The steel drywell head is the weak link as concluded in Appendix B.8 of the PRA report.

DCD Impact

No DCD changes will be made in response to this RAI.

NRC RAI 19.2-41, Supplement 1

NRC Assessment Following the February 5, 2007 Audit

Staff Assessment

a) Acceptable.

b) To address SECY 93-087, the pressure and temperature transients which are associated with the more likely severe accident challenges should be defined. See Staff Assessment in c) and d) of RAI Number 19.2-39 above.

In addition, DCD Section 6.2.5.4.2 should be cross referenced in the appropriate section of DCD Chapter 19, for deterministic containment performance assessment.

c) While acknowledging that no data exist for over-pressurization of containment structures similar to the ESBWR design (with more geometric discontinuities than typical containments in the current fleet of reactors) at both ambient and severe temperature environments, GE provided a summary of the state of available containment tests and insights inferred from the test results regarding the ultimate internal pressure capacity of pre-stressed and reinforced containment, which are consistent with the findings provided in NUREG/CR-6906, "Containment Integrity Research at Sandia National Laboratories." Given the lack of applicable experimental data, the staff will have rely on the ANSYS analyses GE conducted to estimate the pressure capacity of the containment. The staff is concerned with that the effects of elevated concrete temperature has not been appropriately addressed.

Audit Interest

Discuss and resolve how GE will address SECY 93-087 with respect to deterministic containment performance analysis. Review GE's calculations of the containment internal pressure capability (Containment components include: Wetwell, Upper Drywell, Pedestal, Basemat Drywell Head and PCCS heat exchangers) in accordance with ASME Service Level C or Factored Load limits at the severe accident temperature (500°F?).

Status Update/Resolution of RAI

b) Same as 19.2-39, d) above.

c) GE will redo both containment pressure performance analysis solely based on the new analysis performed using the 3-D ABAQUS ANACAP-U model with the pressure and temperature profiles which the staff found to be appropriate, except for the temperature of 43.3°C specified for the drywell head. GE will provide a justification for using 43.3°C for drywell head.

The new analysis will be used to determine the containment pressure fragility and associated failure locations for all the structural components comprising the containment pressure boundary.

The new 3-D ABAQUS model will also be relied upon for determining the Level C pressure capacity of all the structural components comprising the containment pressure boundary, except for the drywell head and its anchorage, as well PCCS head exchanger, the Level C capacity of which will be determined using ASME Code Section III. However, the ABAQUS will be used to verify that the drywell head pressure capacity for the ESBWR design will not be governed by asymmetric buckling, but controlled by axisymmetric plastic yielding of the crown.

GE's PRA Section 8 and DCD Chapter 19 will be revised to reflect the changes in both deterministic (Level C) and fragility analyses as a result of the application of the new ABAQUS model.

GE will provide NRC with revised material describing the ABAQUS analysis.

GE Response

b) See Item c below and response to Item d in RAI 19.2-39 S1.

c) On Section 1.4.4, p. I.41 of SAT report it was stated that the internal temperature of the UDW head under a DCH scenario would be bounded by 450 K. This is easy to demonstrate.

In Table 5.3-1 of the DCD we find that the upper head insulation is designed so that the maximum heat loss under normal operating conditions is 682 kJ/m^2h which amounts to 189 W/m^2. If this is taken to occur at a temperature difference of 237 K (i.e., 560-323, where 560 K is the RPV steam temperature at normal operating conditions, and 323 K is the gas temperature in the upper head region also at normal operating conditions), and if we take a maximum temperature difference just prior to DCH of 777 K (i.e., 1,100-323), the above value of the heat flux can be rescaled by the ratio of the driving forces (3.28) to ~600 W/m^2. [Note that the 1,100 is a maximum since a still higher temperature would lead to spontaneous depressurization and no DCH].

So the question translates to what temperature difference is needed across the 40 mm of the carbon steel UDW head to accommodate this level of the heat flux. The thermal conductivity of carbon steel is ~40 W/m K, so we find:

$\Delta T = 600\ W/m^2\ 40\ 10^{-3}\ m / 40\ W/m\ K = 0.6\ K$

This means that the thermal environment of the UDW head will remain unchanged.

A pressure fragility analysis is performed using the ABAQUS/ANACAP-U software and detailed 3D finite element modeling. This will be documented in Appendix 19C in Rev 3 of the DCD Tier 2. All failure modes of all components in the primary containment system are considered for a range of thermal conditions representing different accident scenarios. The modeling methods and analysis procedures employed are summarized in Attachment 1, which is an updated version of the GE presentation in the NRC audit meeting. As discussed in RAI 19.2-39 a), this modeling is also used to provided a

deterministic analysis for demonstration of RCCV integrity for SECY-93-087 and 10 CFR 50.44.

As part of the fragility evaluation, variations on the temperature for the inside surface of the drywell head were considered. An inside temperature of 57°C (135°F) had no effect on the pressure capacity relative to the 43.3°C (110°F) assumed. An inside temperature of 260°C (500 °F) was found to increase the pressure capacity. The pressure capacity of the drywell head is limited by leakage at the bolted flange, which develops because of prying action of the flange and yielding in the bolts. A hotter inner surface temperature helps resist the separation of the flanges on the inner surface because the hot inner surface must expand relative to the colder outer surface. Because the A516 material does not have any significant degradation in ultimate strength or ductility up to this temperature of 260°C (500°F), there is no change in the failure mode. This means it requires a somewhat higher pressure to overcome this thermal induced stress to reach the same flange distortion level to yield the bolts.

DCD Impact

DCD Tier 2 Subsection 6.2.5.4.2 was revised and moved to DCD Tier 2 Appendix 19B for deterministic Level C analysis and was provided in MFN 06-268, Supplement 1. DCD Tier 2 Appendix 19C was revised for probabilistic fragility analysis and was provided in MFN 06-268, Supplement 1.

NRC RAI 19.2-41, Supplement 2

The staff reviewed GEH's response (MFN 06-268 S1, dated April 13, 2007), and seek clarification on Response c) as follows:

(A) The staff determined that the justification for the low temperature boundary condition for the drywell head (43.3° C or 110°F) under the accident condition is insufficient.

In the original containment fragility analysis as documented in GEH PRA report, Revision 1, Appendix B.8, GE specified the accident steady-state temperature of 260° C (500° F) for the drywell airspace and drywell head shell (neglecting the cooling effect of the pool above the head). During the staff's February 5-7, 2007 on-site audit, GEH informed the staff that GEH will replace the existing containment performance analysis with a new and more technically enhanced 3-D ABAQUS/ANACAP-U finite element analysis. Based on GEH's presentation of the new fragility analysis ABAQUS/ANACAP-U model, the staff considered the approach acceptable. However, the staff identified an issue with the new ABAQUS/ANACAP-U analysis concerning the temperature boundary condition of 43.3° C (110° F) imposed for the drywell head shell, as opposed to the assumption of 260° C (500° F) for the drywell head shell made in the original containment performance analysis. GEH indicated at the staff's February 5-7, 2007 on-site audit meeting that the pool water directly above the drywell head shell will keep the head shell at 43.3° C (110° F). Since the drywell head airspace is only separated from the drywell air space by the bellow which is made of a steel plate, the staff questioned whether the head shell can be kept at 43.3° C (110° F) while the drywell air space is assumed to be at 260° C (500° F).

Consequently, the staff requests the applicant to submit a technically sound and complete justification, possibly through an appropriate heat transfer analysis, for its assumption that the drywell head remains at the normal operating containment atmosphere temperature of 43.3° C (110°F) under the accident condition, while the containment atmosphere is at 260° C (500°F) at steady state.

(B) In addition, the staff determined that the statement in the response,

"A hotter inner surface temperature helps resist the separation of the flanges on the inner surface because the hot inner surface must expand relative to the colder outer surface. Because the A516 material does not have any significant degradation in ultimate strength or ductility up to this temperature of 260°C (500°F), there is no change in the failure mode. This means it requires a somewhat higher pressure to overcome this thermal induced stress to reach the same flange distortion level to yield the bolts,"

requires clarification, and that additional information on the response of the bolted flange connection at elevated temperature is needed. The staff agrees that the above statement may be applicable early in the temperature transient, when there is a significant temperature gradient from the inside surface to the outside surface of the flanges. However, as the transient progresses and the temperature of the bolted flange connection reaches a steady state condition, the effect of elevated temperature may reduce the pressure at which leakage is predicted. The applicant has not addressed this in its response.

Consequently, the staff requests the applicant to:

(1) describe in detail the steady state temperature condition of the bolted flange connection for the accident condition;

(2) identify the coefficients of thermal expansion for the flange material and the bolt material;

(3) discuss o-ring degradation at the accident temperature;

(4) provide a plot showing the average temperature of the flanges and the average temperature of the bolts, from initiation of the transient up to achievement of the steady state condition;

(5) describe the stress and deformation state of the bolted flange connection at the steady state condition; and,

(6) provide the estimate of pressure capacity of the bolted flange connection at the steady state condition and technical basis for the estimate.

(C) GEH indicated at the staff's February 5-7, 2007, on-site audit that the bolt preloads for the major penetrations will be set for the ultimate containment pressure capacity. However, the new containment performance analysis using ABAQUS/ANACAP-U as documented in the proposed DCD Tier 2, Appendix 19B, did not calculate the containment Level-C pressure capacity; rather it demonstrated that the containment Level-C pressure capacity will be higher than the pressure loads induced by the more likely containment accident scenarios and the 100% MWR. Therefore, GEH needs to stipulate quantitatively in Tier 2 the bolt preloads for the major penetrations including the drywell head, which were used in the ABAQUS/ANACAP-U analysis.*

GEH Response

(A) The temperature of the inner surface of the drywell head during the most likely accident scenario was previously based on physical separation between the drywell airspace and the space directly under the drywell head. Based on venting channels between these airspaces and more detailed MAAP analyses, GEH agrees with the staff position that the space underneath the drywell head may reach 260°C (500°F) temperatures for steady state accident conditions. Furthermore, the previous steady state temperatures of the reactor cavity water pool above the drywell head and the dryer/separator pool above and to the side of the drywell head are revised due to heat flowing across the drywell head. The temperature of the water in these pools is changed from 43°C (110°F) to 100°C (212°F). A new pressure capacity analysis for the drywell head as well as for the RCCV and liner is performed using these new temperature conditions. In both cases, the median values of all parameters are considered to define new median pressure capacities. The uncertainty is assumed to remain as before, that is, no additional analyses with parameter variations are performed to develop new values for the lognormal standard deviations. These new median based analyses are documented in Revision 5 of DCD Tier 2 Appendix 19C. It is also noted that new bolt material and bolt prestress loads discussed in NRC RAI 3.8-118 are incorporated into these new pressure capacity analyses.

(B)

(1) The steady state temperature condition of the bolted flange connection for the 260°C (500°F) steady state accident condition is described in detail in DCD Tier 2 Appendix 19C. The inner surface of the drywell head is maintained at 260°C (500°F) while the outer surface of the drywell head and bolted flanges are kept at 100°C (212°F). High heat transfer coefficients on these surfaces are used to enforce the atmospheric and water temperatures on the inner and outer surfaces, respectively. A steady state thermal analysis is performed to establish the temperature distributions in the material interior of the exposed surfaces.

(2) The coefficient of thermal expansion used for the flange material (SA-516 Gr 70) is 1.17E-5 m/m/°C (6.5E-6 in/in/°F), and for the new bolt material (SA-437 Grade B4B) is 1.08E-5 m/m/°C (6.0E-6 in/in/°F).

(3) The O-ring is assumed fully degraded at 260°C (500°F) accident temperature and no credit is taken in the capacity analysis for the leakage integrity of the bolted flange. Leakage is prevented by full contact around the toe of the flanges due to the prying action until bolt yielding develops.

(4) The analysis is based on a steady state thermal condition. A transient thermal analysis is not performed, and thus temperature history plots from initiation of the transient up to achievement of steady state condition are not available.

(5) The stress and deformation state of the bolted flange connection at steady state is described in DCD Tier 2 Appendix 19C. The internal pressure induces a prying action in the flanges as separation along the inner surface or heal develops. This produces a high compressive load outboard of the O-rings around the toe of the flanges, and eventually the bolts will yield in tension.

(6) The estimate of the pressure capacity of the bolted flanges is 1.426MPaG (4.60 times the design pressure) for the 260°C (500°F) steady state accident condition. The 95% High Confidence value of the pressure capacity is 1.095MPaG (3.53 times the design pressure) for the 260°C (500°F) steady state accident condition. This includes the new temperature conditions and the new bolt material and bolt prestress loads. The technical basis for the estimate is the detailed, non-linear structural analysis as described in the attached DCD Tier 2 Appendix 19C, Revision 5 markup.

(C) The bolt preloads for the drywell head, equipment hatch and wetwell hatch will be designated as Tier 2* information in DCD Tier 2 Figures 3G.1-51, 3G.1-52 and 3G.1-53.

DCD/NEDO-33201 Impact

DCD Tier 2 Appendices 19B and 19C and Figures 3G.1-51, 3G.1-52 and 3G.1-53 will be revised in DCD Revision 5 as noted in the attached markups.

No change to NEDO-33201 is required in response to this RAI Supplement.

NRC RAI 19.2-86

The new ABAQUS/ANACAP-U analysis result as presented in DCD, Tier 2, Revision 4, Appendix 19B, showed that at an internal pressure of 0.987 MpaG (MWR pressure), or 3.18P_d, the strain in the liner of the upper drywell wall at the connection with the top slab reached 0.72%, which exceeded the factored load limit for liners (0.3% tensile membrane strain, ASME Section III, Div 2, CC-3720). Based on Figure 19B-5 of DCD, Tier 2, Revision 4, Appendix 19B, the staff estimated that the containment Level capacity slightly less than 2.5 P_d with respect to the Code Allowable, controlled by the failure mode of the liner strain at Location A. Therefore, the requirement of 10 CFR 50.44(c)(5) is not met. The staff also disagrees with the characterization of DCD, Tier 2, Revision 4, Appendix 19B that the containment Level C pressure capacity can be estimated using 99-percentile fragility value, because the Level C allowable is a design parameter that was not derived on a fragility basis.

GEH further qualitatively justified that the liner strain could be reduced to within the factored load limit by accounting for the thermal induced strain, which is not consistent with the requirement of R.G. 1.7. Also, based on Figure 19B-5 of DCD, Tier 2, Revision 4, Appendix 19B, the excess liner strain appears to be a localized phenomenon (designated as location A in the figure). To facilitate the staff's evaluation, please provide:

a) whether the strain at location A of Figure 19B-5 was calculated based on membrane or membrane plus bending (if the strain is due to membrane plus bending, the code allowable factored load limit is 1%);

b) time histories of pressure and temperature on the liner due to WMR and a summary of thermal analysis which reduces the strain induced by the internal pressurization;

c) SRP 3.8.1, II, SRP Acceptance Criteria 4.K.i for computing ultimate pressure capacity of concrete containment states that "One acceptable methodology for cylindrical reinforced concrete containment is to estimate the capacity based on attaining a maximum global membrane strain away from discontinuities of 1 percent." Please assess if there could be a change in failure mode if 1% strain is used as the failure criteria for liners in place of Table 19C-5 of DCD, Tier 2, Revision 4, Appendix 19C.

GEH Response

a) The liner strain calculated at the connection of the RCCV wall to the top slab contains both membrane and bending components. The excess liner strain is indeed a localized phenomenon occurring at 4 locations where large stiffness discontinuities exist at the RCCV to top slab connection due to the connections with the main pool girders. The code allowable factored load limit of 1% liner strain for membrane plus bending will be used for the calculated liner strain at these locations for the revised Level C calculations in DCD Tier 2 Appendix 19B, Revision 5.

b) The analysis to meet the Level C pressure capacity for 100% Water Metal Reaction (WMR) is not based on time histories of pressure and temperatures applied to the liner. The Level C capacity analysis applies dead load and then statically increments internal pressure up to the pressure corresponding to 100% WMR (0.987 MPaG). The side calculation to evaluate the effects of temperature on the liner strain used the temperature distributions from the 260°C

(500°F) steady state thermal conditions developed for the fragility analysis in DCD Tier 2 Appendix 19C. These temperatures were incrementally applied (starting from the ambient normal operating thermal conditions) along with the design pressure, and then the temperatures were frozen, and the internal pressure incrementally increased to that corresponding to 100% WMR. The Level C calculation with thermal was identical to the 260°C (500°F) steady state fragility analysis except the material properties were lower bound design values for the Level C analyses. The new Level C calculation reported in DCD Tier 2 Appendix 19B, Revision 5, will only be that for pressure and dead load. No side calculations to evaluate the effects of thermal strain will be included in the revised calculations.

c) The new pressure fragility analyses discussed in NRC RAI 19.2-41, Supplement 2 are further evaluated to assess if there could be a change in failure mode if 1% global membrane strain is used as the failure criteria for liners in the fragility analysis. In the global model analysis for pressure capacity of the RCCV and liner using median values of parameters, a pressure capacity of 1.645 MPaG (5.30 times design pressure) is established. This capacity is limited by liner tearing at the connection of the RCCV and top slab where the local liner strain calculated is compared to the failure criteria established in DCD Tier 2 Table 19C-5. Figure 19.2-86(1) plots the hoop liner strain in the cylindrical portion of the RCCV away from discontinuities for the same analysis conditions. At 5.30 times the design pressure, the global liner membrane strain in the cylindrical portion of the RCCV away from discontinuities is found to be less than 0.25 %. Using a criterion of 1% global membrane strain would result in calculating a pressure capacity for the RCCV of greater than 9 times design pressure. If 1% global membrane strain is used as the failure criteria for liner tearing, then the ranking of leakage due to liner tear in the RCCV would shift to be after RCCV structural failure due to shear failure in the pool girders.

DCD/NEDO-33201 Impact

DCD Tier 2 Appendices 19B and 19C will be revised in DCD Revision 5 as noted in the attached markups.

No change to NEDO-33201 is required in response to this RAI.

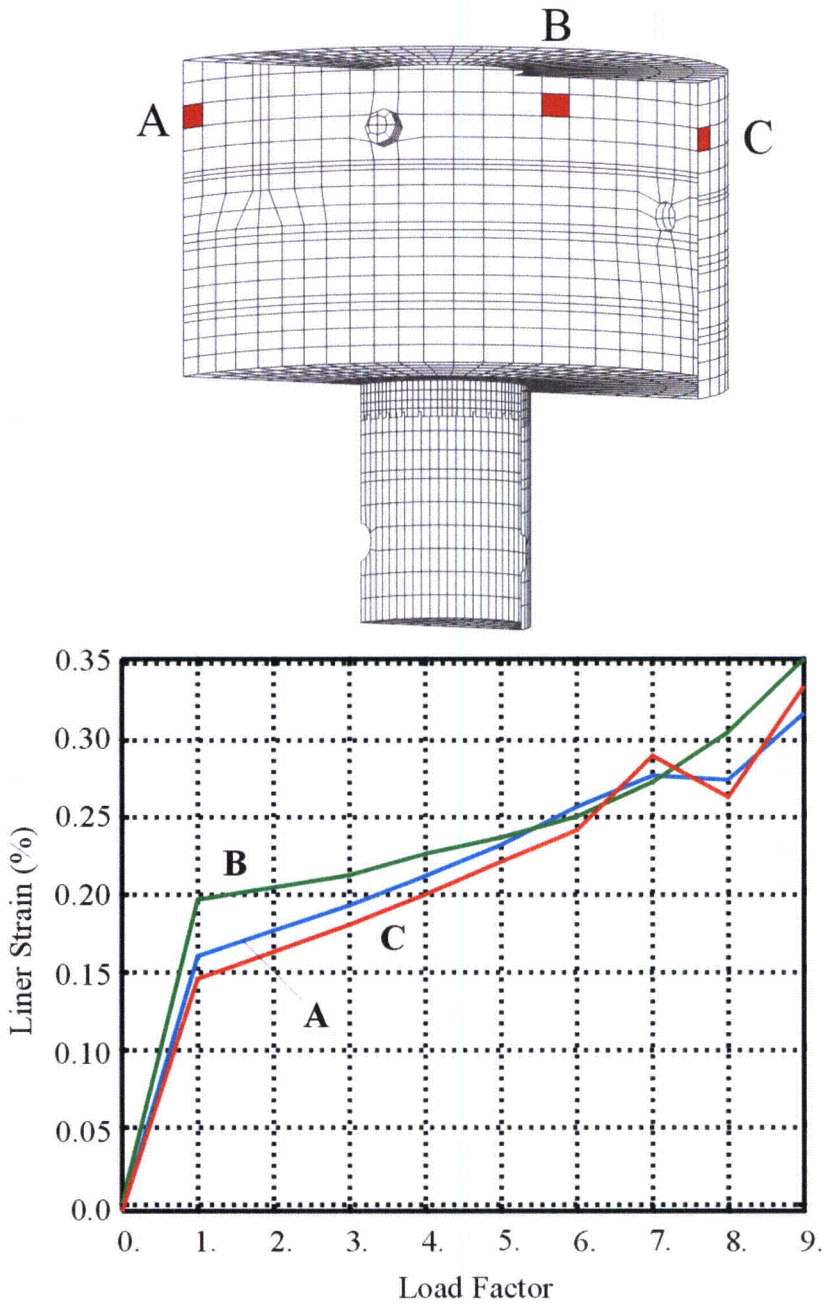

Figure 19.2-86(1) Liner Hoop Strains at Far Field, 260°C (500°F) Steady State, Median Values

19B. DETERMINISTIC ANALYSIS FOR CONTAINMENT PRESSURE CAPABILITY

19B.1 INTRODUCTION

This Appendix presents the deterministic analysis performed and results obtained for the containment ultimate capability under internal pressure in accordance with requirements in 10 CFR 50.44(c)(5) and SECY-93-087.

10 CFR 50.44(c)(5) states "An applicant must perform an analysis that demonstrates containment structural integrity. This demonstration must use an analytical technique that is accepted by the NRC and include sufficient supporting justification to show that the technique describes the containment response to the structural loads involved. The analysis must address an accident that releases hydrogen generated from 100 percent fuel clad-coolant reaction accompanied by hydrogen burning. Systems necessary to ensure containment integrity must also be demonstrated to perform their function under these conditions". RG 1.7 Revision 3 provides an acceptable method for demonstration of containment structural integrity in meeting the ASME Section III acceptance criteria as follows:

- That steel containments meet the requirements of the ASME Boiler and Pressure Vessel Code (Edition and Addenda as incorporated by reference in 10 CFR 50.55a(b)(1)), Section III, Division 1, Subarticle NE-3220, Service Level C Limits, considering pressure and dead load alone (evaluation of instability is not required); and
- That concrete containments meet the requirements of the ASME Boiler and Pressure Vessel Code, Section III, Division 2, Subarticle CC-3720, Factored Load Category, considering pressure and dead load alone.

SECY-93-087, item J states "The containment should maintain its role as a reliable, leak-tight barrier by ensuring that containment stresses do not exceed ASME service level C limits for a minimum period of 24 hours following the onset of core damage, and that following this 24-hour period the containment should continue to provide a barrier against the uncontrolled release of fission products."

Both sets of requirements are satisfied by performing a deterministic analysis, termed "Level C Evaluation", to ensure that the Level C or Factored Load pressure capability of the containment structure is no less than 0.987 MPaG (143 psig) generated from 100 percent fuel clad-coolant reaction nor 0.62 MPaG (90 psig) resulting from more likely severe accident challenges, taking into account temperature effect on the material strength. The representative severe accident temperature considered is 260°C (500°F). The pressure units MPaG used in this appendix are gauge pressures unless noted otherwise.

The current Level C analysis provided herein is based on the updated temperature conditions used for the pressure capacity fragility described in more detail in Appendix 19C. The global analysis for the Level C capacity check for the RCCV and Liners is updated for the new temperature conditions in the airspace under the drywell head, 260°C (500°F), and in the water in the reactor well and the equipment storage pool, 100°C (212°F), associated with the 260°C (500°F) steady state accident condition.

elements representing the soil foundation. Solid (20-node continuum) elements with reduced Gaussian quadrature integration are used to model the reinforced concrete sections. The reinforcement bars are modeled as embedded, truss-like steel elements at the appropriate locations within the concrete elements. Membrane elements (plate elements without bending stiffness) are generally used to model the steel liners. These elements are attached to the nodes of the concrete elements for compatibility with the concrete deformations. This assumes that the liner anchorage system keeps the liners in contact with the concrete for this global modeling of the RCCV performance. Some plate bending elements are used for the thickened sections at connections. Representations for the large equipment hatches, personnel airlock penetrations, and the drywell head components are included using plate bending elements. Plate bending elements are also used to model the steel components of the internal structures, including the vent wall, diaphragm floor, reactor vessel shield wall, and the reactor pressure vessel support brackets.

The material properties used for the Level C analysis correspond to minimum design values. The structural properties are dependent on temperature and are summarized in the following tables. Table 19B-2 provides a summary of the elastic properties for steels, and Table 19B-3 provides a summary of the plastic properties of the steel materials. Table 19B-4 provides a summary of the concrete properties. All thermal properties are assumed to be constant with temperature and are summarized in Table 19B-5.

19B.2.3 Analysis Results

~~The analysis is completed to a load factor of 3.5 times design pressure or an equivalent internal pressure of 1.085 MPaG (157.5 psig).~~ Figure 19B-2 plots contours of the minimum principal stress in the concrete at 0.992 MPaG (144 psig) or a load factor of 3.2 times design pressure to illustrate the concrete compressive stress distribution. This plot identifies the locations of elevated concrete stresses in 4 areas; a) on the RCCV wall below the suppression pool floor connection, b) on the bottom of the top slab around the drywell head opening, c) on the top surface of the top slab at the RCCV walls, and d) at the outside connection of the pedestal wall with the basemat. The peak compressive stresses identified in the plot are on the top surface of the top slab under the PCCS pool walls ~~where the temperature is at ambient levels.~~ Figure 19B-3 plots contours of the maximum principal strain in the concrete at 0.992 MPaG (144 psig) or a load factor of 3.2 times design pressure to illustrate the areas of concrete cracking and potential elevated rebar stresses. This plot indicates that the critical area for this loading is at the connection of the RCCV wall to the top slab and to a lesser extent at the connection of the RCCV wall to the suppression pool slab.

Table 19B-6 provides a summary of the maximum rebar and concrete stresses and the associated ratio to the ASME Level C (factored load) allowable limits at an internal pressure of 0.62 MPaG (90 psig) corresponding to the most likely severe accident conditions. All concrete and rebar stresses are found to be well below the ASME allowable limits for this pressure in accordance with the requirements of SECY-93-087.

Figure 19B-4 plots contours of maximum principal strains in the liner at 0.992 MPaG (144 psig) or 3.2 P_d. This plot has the maximum strain contour value set to 0.3% corresponding to the ASME factored load allowable for membrane tension to identify the critical areas. The critical areas are at the RCCV wall connection with the suppression pool floor slab and at the connection

with the top slab. Examination of individual element strains indicates that the 2 most critical areas are at the connection of the RCCV wall to the top slab under the location where the upper pool girders are connected across the top slab. Figure 19B-5 plots the maximum principal strain versus pressure at ~~representative elements for these critical locations~~ these two locations near these stiffness discontinuities, identified as points ~~A, B and C~~ A and D in the figure. This peak strain includes membrane and bending and meets the 1% allowable limit. Figure 19B-6 plots the membrane strain in the liner at other representative points away from these discontinuities. This plot shows that the liner membrane strain remains below the allowable of 0.3% for an internal pressure of 0.987 MPaG (143 psig) pressure corresponding to 100% fuel clad-coolant reaction even for the locations at the top slab connection but away from the discontinuity. ~~All liner strains easily meet the ASME strain limits for 0.62 MPaG (90 psig) pressure or a load factor of 2.0 P_d. This plot shows that the liner at the connection with the suppression pool slab (Point B) meets the ASME factored load limit of 0.3% membrane strain at 0.987 MPaG (143 psig) pressure corresponding to 100% fuel clad coolant reaction.~~ All liner strains easily meet the ASME strain limits for 0.62 MPaG (90 psig) pressure or a load factor of 2.0 P_d. ~~Point C is a representative typical location for the liner at the connection with the top slab, and Point A is at a local concentration that develops at the locations where the upper pool girders connect to the top slab. Figure 19B-6 plots the maximum principal (EP2) and plastic (PEEQ) strains at this local concentration in the RCCV wall liner at the top slab connection. Yielding of the liner at this local concentration just starts at the 0.62 MpaG (90 psig) pressure level. At an internal pressure of 0.987 MpaG (143 psig) or 3.18 P_d, the plastic strain in the liner for this location reaches 0.72%. While this exceeds the ASME factored load limit, this value is still on the shoulder of the stress-strain curve, as illustrated in Figure 19B-7. This level of plastic strain is well below the ductility limit, even considering substantial strain concentration factors, and, in addition, this strain is due to a localized effect.~~

~~Furthermore, because the liner will undergo compression when exposed to the temperatures that accompany this accident pressure, the level of membrane tension strain will be reduced. When thermal induced stresses are also included, the maximum liner strain at this location reduces to 0.25% at 0.987 MpaG(143 psig), as illustrated in Figure 19B-8. Thus, if the thermal stress is included, then the liner strain is within the factored load limit even at the local concentration for the 100% fuel clad coolant reaction pressure.~~ Thus, it is demonstrated through the nonlinear analysis that the liner remains a leak tight barrier for 0.987 MPaG(143 psig) pressure corresponding to 100% fuel clad-coolant reaction and meets the requirements of 10 CFR 50.44.

While not a requirement of 10 CFR 50.44, the peak rebar and concrete stresses along with the ratios to ASME factored load allowable limits are summarized in Table 19B-7 for a pressure of 0.992 MPaG(144 psig) or a load factor of 3.2 P_d. All concrete compressive stresses remain below the ASME allowable limit at this pressure level. The same local area identified in the liner strains shows some slight yielding in the rebar at this pressure level. These are the inner vertical bars in the RCCV wall and the bottom horizontal bars in the top slab at this connection, but only for a local area under the connection of the upper pool girders with the top slab. The table also identifies the maximum plastic strain levels found in the rebars for these locations. The largest plastic strain is 0.3940 %, which is almost within the ASME limit for liner membrane strain. Again, the peak response of these local rebars is just past the 0.2% yield and still well on the shoulder of the stress-strain curve. This level of plastic strain is well below the failure level

for reinforcement steel, and the nonlinear analysis confirms the integrity of the RCCV walls and liner at this pressure level.

19B.2.4 Summary

The deterministic finite element analysis demonstrates that the RCCV and liner maintain structural integrity and provide a leak tight barrier per the requirements of SECY-93-087 for internal pressure corresponding to the most likely severe accident challenges and per the requirements of 10 CFR 50.44(c)(5) for pressures corresponding to 100% fuel clad-coolant reaction. The analysis uses lower bound material properties, including degradation with temperature. The modeling is consistent with the pressure fragility analyses in Appendix 19C, accounting for nonlinear material response, such as concrete cracking in tension with reduced shear stiffness, concrete yielding and strain softening in compression, and steel yielding and strain hardening in compression or tension. The concrete and rebar stresses and the liner strains remain within the ASME factored load allowable limits for 0.62 MPaG (90 psig) per the requirements of SECY-93-087. The concrete stresses also remain within the ASME allowable limit for factored load level even at 0.987 MPaG (143 psig) pressure. The liner strains ~~including thermal effects~~ are within the factored load allowable at 0.987 MPaG (143 psig). Some slight yielding of rebar develops at the 0.987 MPaG (143 psig) pressure level in local areas. It is thus demonstrated that the structural integrity of the RCCV and liner system is maintained for the more likely severe accident challenges and for the scenario for pressures generated from 100% fuel clad-coolant reaction.

~~An estimate of the actual Level C pressure capacity can be determined from the fragility analysis described in Appendix 19C, which includes the thermal stress for the 260°C (500°F) steady state thermal condition. Using $\beta = -2.33$, a 99% confidence level for the pressure capacity for the RCCV and liner system is determined to be 1.185 MPaG (172 psig). It is also noted that the fragility analysis determined that the 99% confidence level for leakage at the bolted flange connection of the drywell head is a pressure level of 1.097 MPaG (159 psig)~~ An estimate of the actual Level C pressure capacity is determined using Figures 19B-5 and 19B-6 to find the internal pressure where the calculated liner strains reach the ASME allowable limits. Both the 1% strain for membrane plus bending at the discontinuity and the 0.3% hoop membrane strain away from discontinuities are reached near the same load factor. Thus, the Level C pressure capacity of the RCCV and Liner system is established at a load factor of 3.26 times the design pressure or 1.011 MPaG (146.5 psig) based on the deterministic design-based analysis.

19B.3 DRYWELL HEAD

Level C pressure capability of the drywell head is evaluated for pressure retaining parts (sleeve/torispherical head), bolted flange and anchor structures (flange plates/gusset plates).

The basic equation for Level C pressure capability is:

$$P_c = (S_c - \sigma_d) / \sigma_{up} \qquad (19B\text{-}1)$$

where:

P_c = Level C pressure

S_c = Level C allowable stress at temperature 260°C (500°F)

σ_d = Stress due to dead load

σ_{up} = Stress due to unit pressure, 1 MPaG (145 psig)

Pressure retaining parts (sleeve and torispherical head) are evaluated based on the primary membrane stress Pm applying ASME Section III NE-3324, in which the maximum allowable stress S is taken to be Sy (material yield strength at temperature) as Level C stress limit in accordance with NE-3220. The local membrane stress PL and local membrane plus primary bending stress PL + Pb are non-controlling. Dead load (self-weight and hydrostatic pressure of the reactor well) is conservatively neglected.

The Bolted flange is evaluated in accordance with ASME Section III, Division 1, Appendix XI. The average of longitudinal hub stress and radial flange stress, which is the severest stress among the ones stipulated in article XI-3250, and the flange bolt stress stipulated in article XI-3220 of Appendix XI and Subsection NE-3230 are evaluated. Dead load is conservatively neglected.

Anchor structures (flange plates and gusset plates) are evaluated based on stress intensity applying ASME Section III NE-3221. Concrete compressive stress is evaluated in accordance with ASME Section III Division 2 CC-3421.1 for factored load limit. Dead load including reactor well hydrostatic pressure is considered for the evaluation of Level C capability of anchor structures.

The Level C pressure capabilities of each part of the drywell head are summarized in Table 19B-9. The governing pressure is 1.033 MPaG (150 psig), which is controlled by the lower flange plate of the anchorage.

19B.3.1 Buckling Analysis

An evaluation for the buckling capacity of the drywell head was analyzed using the ABAQUS finite element program (Reference 19B-2). An elastic-plastic analysis was analyzed including the effects of gross and local buckling, geometric imperfections, material nonlinearities, and large deformations as allowed in NE-3222 (Reference 19B-1) for establishing buckling stress values of torispherical heads. This analysis is used to determine the pressure capacity and the failure mode, whether due to buckling under compressive hoop stress in the knuckle or due to tensile plastic failure in the dome region above the knuckle. ~~The finite element model for the torispherical head including the top flange is shown in Figure 19B-9. This analysis was conducted before the latest revision to strengthen the bolted flange connection using thicker flanges and the tapered shell sections connecting to the flanges. However, this change will have very little affect on the buckling analysis because the buckling analysis assumes that the top flange is fixed. The critical areas are in the knuckle region above the tapered shell section and in the apex of the dome region where the shell thickness is unchanged at 40 mm.~~

The first step in the analysis is to confirm and demonstrate that the torishperical head is modeled with sufficient resolution and that the analytical procedure is capable of capturing the buckling failure mode from compressive hoop stress in the knuckle region. To this end, a benchmark analysis was performed using the drywell head model, but modifying the thickness of the shell to simulate a torispherical shell configuration that exhibited this buckling failure mode when tested. The finite element model for the torispherical head including the top flange for this benchmark buckling study is shown in Figure 19B-7. The thickness of the shell elements in the analysis model was reduced so that the D/t ratio matches that of a tested configuration reported in

Reference 19B-4. The model is then clamped along the flanges, and an internal pressure load is incrementally applied until failure occurs in the analysis. The analysis model clearly predicts buckling failure at the same internal pressure where buckling occurred in an experimental test of a similar configuration. The analysis model considers a 10.4 m (34.12 ft) diameter torispherical head, based on the ESBWR design, but with the shell thickness reduced so that the diameter to thickness ratios match that of a tested configuration having a 4.92 m (16.14 ft) diameter. The parameters for the analysis model and the tested shell configuration are summarized in Table 19B-8, along with the comparison of the calculated and measured pressure causing buckling.

Figure 19B-~~10~~8 plots the crown deflection to shell thickness ratio versus the load and shows the sudden snap back indicative of bifurcation type buckling failure. It is noted that torispherical heads can sustain significantly more internal pressure than that causing the first buckle in the knuckle region as reported in Reference 19B-6. However, when the buckles develop, there is a temporary instability due to sudden volume change and sudden large changes in the material response, and these effects generally cause the numerical instability in the analysis. Figure 19B-~~11~~9 plots the plastic strain contours for the buckled shape predicted by the analysis model. This benchmark analysis is in good agreement with experimental test data in predicting pressure causing buckling in the knuckle. Thus, it is concluded that the modeling has sufficient resolution and the analytical procedure employed has the required capability to capture buckling failure modes in the analyses for pressure capacity of the torispherical drywell head.

An analysis for the pressure capacity of the ESBWR drywell head configuration is thus performed using the design thickness of 40 mm (1.57 in) for the torispherical shell. This gives a value of 262 for the D/t parameter of the actual drywell head. Figure 19B-10 shows the finite element model used for the buckling analysis of the ESBWR drywell head. This model retains the same finite element mesh that was qualified in the buckling study above, but adds the tapered barrel section and flange thickness corresponding to the latest design configuration for the ESBWR drywell head. The analysis uses the lower bound or design values for the steel properties, ~~-~~evaluated at 260°C (500°F), namely yield strength = ~~262~~212.4 MPa (~~38~~30.8 ksi), tensile strength = 483 MPa (70 ksi), and minimum required elongation of 17%. The model is clamped along the bottom of the flange, and the internal pressure is incrementally increased to find the true pressure capacity. This analysis is performed at ~~an ambient temperature of 15.5°C (60°F)~~ 260°C (500°F) and includes the external hydrostatic pressure of the water on the top of the head. Figure 19B-~~12~~11 provides a plot of the crown deflection as a ratio of the shell thickness for the increasingly applied internal pressure load. The load factor is the multiplier on the design pressure of 0.31 MpaG (45 psig). Also indicated on this figure is the procedure described in Reference 19B-5 for identifying the axisymmetric yielding pressure, P_{c2}, developed from studies using the BOSOR 5 computer program on a wide range of test configurations. Basically, the procedure is to find the value for d/t at first yield (point a), then take double this value for the same load (point b), draw a line through this point from the origin to intersect the displacement curve (point c), and read the corresponding pressure load (point d). This axisymmtric yield pressure is the internal pressure at which plastic yielding in the crown of the shell initiates leading to plastic failure of the shell. However, as noted in Reference 19B-5, P_{c2} is typically well below the actual failure pressure. As shown in the figure, the ABAQUS elastic plastic analysis calculates a similar but slightly higher value for this initiation of tensile yielding and also indicates that the shell still has significant reserve strength after the initiation of yielding

in the crown. This analysis confirms that buckling in the knuckle region due to hoop compressive stress does not develop for the as-designed thickness of the drywell head.

To determine the pressure capacity of the drywell head due to tensile rupture in the dome, the pressure is incrementally increased until the strains reach the ductility limit of the material. In the dome, the material is under 1:1 biaxial tensile loading, and the ductility is limited to 50% of the elongation data determined from uniaxial specimens. The specified minimum elongation for A 516 Grade 70 material is 17% at ambient temperatures. This elongation reduces slightly (16.4%) up to temperatures of 260°C (500°F), then increases to about 24% at 538°C (1000°F). For this evaluation, the ductility or failure limit for the material is taken to be a plastic strain of 8%. Because the mesh is adequate (able to capture buckling) and there are no discontinuities in the region where failure will occur, no strain concentration factor for mesh fidelity is required. Figure 19B-~~13~~-12 plots contours of the equivalent plastic strain at mid-thickness for increasing internal pressure to illustrate the plastic deformations leading to tensile rupture in the dome. Initial yielding develops in the knuckle due to hoop compression and meridional tension. Once buckling in the knuckle is avoided, yielding and plastic deformations then concentrate in the dome due to biaxial tension "ballooning" in the dome and apex. At a load factor near ~~1~~4~~1~~5, the ductility limit of 8% strain is reached and rupture of the dome will occur.

In previous analyses considering the torispherical head buckling study, t~~T~~he pressure capacity analysis was repeated considering initial imperfections in the geometry of the shell. The magnitudes of the geometric imperfections considered are based on the maximum allowed imperfections provided in NE-4222.2 of Reference 19B-1, namely that the shell surface shall not deviate outside the specified shape by more than 1-¼ % of the head diameter or inside the specified shape by more than 5/8 % of the diameter. While it is most likely that these minimum and maximum deviations will only occur in 1 or 2 locations around the shell surface, as found in Reference 19B-6, a cosine type shape with 6 peaks in the half model was constructed. This evaluates whether such imperfections could trigger buckling in the knuckle region and change the mode of failure. The assumption is that the closer the imperfections are to the buckling shape, the more likely the chance that the imperfections could trigger the buckling. This analysis also confirmed that buckling did not develop for the actual drywell head configuration even in the presence of these assumed imperfections. ~~In addition, an analysis was also performed using the perfect geometry but considering a temperature of 171°C (340°F) to evaluate the effect of elevated temperature on the pressure capacity. This analysis assumed that the drywell head is free to expand with temperature and that the elevated temperature is uniform across the thickness. Thus, no thermal induced stress is present, and any effect on the pressure capacity is caused by reduction in the material properties.~~

Figure 19B-~~14~~-13 plots the mid-thickness plastic strain in the crown with increasing pressure for ~~for these three analysis cases, namely, perfect geometry at ambient temperature, imperfect geometry at ambient temperature, and perfect geometry at elevated temperature.~~ the analysis at 260°C (500°F). ~~The ductility limit for strain that will cause tearing of the head is also shown on the figure. The failure pressure for perfect geometry at ambient temperature is seen to be a load factor of 13.9 on the design pressure with a reduction to 13.2 P_d for the imposed imperfections. Note that the imposed imperfections did not trigger buckling response in the knuckle. For the perfect geometry at elevated temperature, a pressure of 12.4 P_d would cause tensile failure in the~~

~~dome.~~ Allowing for some conservatism, the pressure capacity for the drywell head is established at 12 P_d or an internal pressure of 3.72 MPaG (540 psig).

In summary, this analysis confirms that the drywell head will not buckle prior to tensile failure in the dome.

19B.4 HATCHES AND AIRLOCKS

Level C pressure capabilities of hatches and personnel airlocks were evaluated for pressure retaining parts (sleeve/head for hatches, sleeve only for airlock), bolted flanges of hatches, sidewalls of airlocks and anchor structures (flange plates/gusset plates).

The basic equation for determining Level C pressure capability is same as the drywell head described in Section 19B.3; however, stresses of hatches and air locks caused by dead load are small are negligibly small.

Pressure retaining parts are evaluated in a manner similar to the drywell head.

Bolted flanges of hatches are evaluated based on the stress analysis result applying ASME Section III, Division 1, Appendix XI and Subsection NE-3221.

Sidewalls of airlocks and anchor structures are evaluated based on stress intensity applying ASME Section III NE-3221.

The Level C pressure capabilities of each part of the hatches and airlocks are summarized in Table 19B-10. The governing pressure is 1.047 MpaG (152 psig), which is controlled by the inside gusset plate of the equipment hatch anchorage.

19B.5 PENETRATIONS

The most critical of the RCCV penetrations are the main steam pipe penetrations. They have the largest flued head and anchor sleeves. Considering the loads transmitted by the main steam pipes, the maximum Level C pressure capability at temperature of 260°C (500°F) is 3.38 MPaG (490 psig).

19B.6 PCCS HEAT EXCHANGERS

The PCCS heat exchangers are part of containment boundary. The Level C pressure capacity at temperature of 260 C (500 F) of the most critical component in the PCCS heat exchangers is 1.33 MPaG (193 psig).

19B.7 SUMMARY

The Level C or Factored Load Category pressure capacities of various components of the containment structure are summarized in Table 19B-11. The limiting pressure is ~~1.033~~1.011 MPaG (~~150~~146.6 psig) associated with ~~the lower flange plate of the drywell head anchorage~~ the strain limits in the liner. It is higher than 0.987 MPaG (143 psig) generated from 100 percent fuel clad-coolant reaction and 0.62 MPaG (90 psig) resulting from more likely severe accident challenges.

Table 19B-5
Summary of Thermal Material Properties

Material	Weight Density (MN/m^3)	Specific Heat (J/kg-K)	Conductivity (W/m-K)
Concrete	0.0235	878.64	1.6
Carbon Steel Liner	0.0770	460.24	53.5
Stainless Steel Liner	0.0770	493.71	16.3
Structural Steel	0.0770	460.24	53.5

Table 19B-6
Summary of Maximum Stresses in Rebar and Concrete at 0.620 MPaG (90 psig) Pressure

Location	Maximum Rebar Tension		Maximum Rebar Compression		Maximum Concrete Compression	
	Stress (MPa)	[1]Ratio to Allowable	Stress (MPa)	[1]Ratio to Allowable	Stress (MPa)	[2]Ratio to Allowable
Top Slab					-8.27	0.32
X-Bar Top	63.63	0.17	-20.39	0.05	On top surface under pool girder at RCCV wall	
X-Bar Bot	154.69	0.52	-55.61	0.19		
Y-Bar Top	84.28	0.23	-27.3	0.07		
Y-Bar Bot	181.3	0.62	-54.57	0.19		
RCCV Wall					-10.12	0.39
Vert In	193.11	0.66	-20.79	0.07	At connection with top slab	
Vert Out	53.36	0.14	-16.46	0.04		
Hoop In	24.22	0.08	-10.26	0.03		
Hoop Out	23.07	0.06	-7.01	0.02		
SP Slab					-9.36	0.36
Hoop Top	5.86	0.02	-5.85	0.02	On bottom surface at RCCV wall	
Hoop Bot	13.35	0.04	-0.24	0.00		
Rad Top	117.56	0.40	-24.99	0.08		
Rad Bot	84.14	0.23	-30.67	0.08		
Pedestal Wall					-14.25	0.55
Vert In	8.15	0.03	-49.49	0.17	Outside surface at connection with basemat	
Vert Out	0.02	0.00	-48.52	0.13		
Hoop In	31.65	0.11	-11.66	0.04		
Hoop Out	27.12	0.07	-10.03	0.03		
Basemat					-6.12	0.30
Top Layers	13.81	0.05	-18.56	0.06	Top surface at pedestal wall, [27.6 MPa, (4 ksi) concrete]	
X-Bar Bot	149.37	0.40	-23.23	0.06		
Y-Bar Bot	132.28	0.36	-23.98	0.06		

[1]allowable is 90% of yield; for inner bars, yield = 327.5 MPa; for outer bars, yield = 413.8 MPa

[2]allowable is 75% of fc'; for inner surface, fc' = 25.91 MPa; for outer surface, fc' = 34.48 MPa

Table 19B-7
Summary of Maximum Stresses in Rebar and Concrete at 0.992 MPaG (144 psig) Pressure

Location	Maximum Rebar Tension		Maximum Rebar Compression		Maximum Concrete Compression	
	Stress (MPa)	[1]Ratio to Allowable	Stress (MPa)	[1]Ratio to Allowable	Stress (MPa)	[2]Ratio to Allowable
Top Slab					-21.34	0.83
X-Bar Top	175.97	0.47	-40.52	0.11	0.042% peak plastic strain in horizontal bars at connection with top slab at pool girders	
X-Bar Bot	344.88	1.17	-159.25	0.54		
Y-Bar Top	254.38	0.68	-40.09	0.11		
Y-Bar Bot	339.85	1.15	-167.77	0.57		
RCCV Wall					-27.53	1.06
Vert In	354.41	1.20	-31.45	0.11	0.40% peak plastic strain in vertical bars at top slab under pool girder locations	
Vert Out	231.67	0.62	-37.15	0.10		
Hoop In	142.78	0.48	-32.52	0.11		
Hoop Out	184.63	0.50	-7.27	0.02		
SP Slab					-18.04	0.70
Hoop Top	3.17	0.01	-19.78	0.07		
Hoop Bot	81.25	0.22	-5.45	0.01		
Rad Top	201.65	0.68	-49.23	0.17		
Rad Bot	162.98	0.44	-55.6	0.15		
Pedestal Wall					-26.59	1.03
Vert In	78.17	0.27	-75.1	0.25		
Vert Out	2.69	0.01	-84.32	0.23		
Hoop In	110.41	0.37	-21.99	0.07		
Hoop Out	88.52	0.24	-23.11	0.06		
Basemat					-12.28	0.59
Top Layers	181.55	0.62	-43.57	0.15		
X-Bar Bot	320.38	0.86	-31.16	0.08		
Y-Bar Bot	336.25	0.90	-42.24	0.11		

[1]allowable is 90% of yield; for inner bars, yield = 327.5 MPa; for outer bars, yield = 413.8 MPa

[2]allowable is 75% of fc'; for inner surface, fc' = 25.91 MPa; for outer surface, fc' = 34.48 MPa

Table 19B-11
Summary of Level C/Factored Load Category Pressure Capacity at 260°C (500°F)

Component	Pressure (MPa), gauge
RCCV and Liners	1.011
Drywell Head	1.033
Hatches and Airlocks	1.047
Penetrations	3.38
PCCS Heat Exchangers	1.33

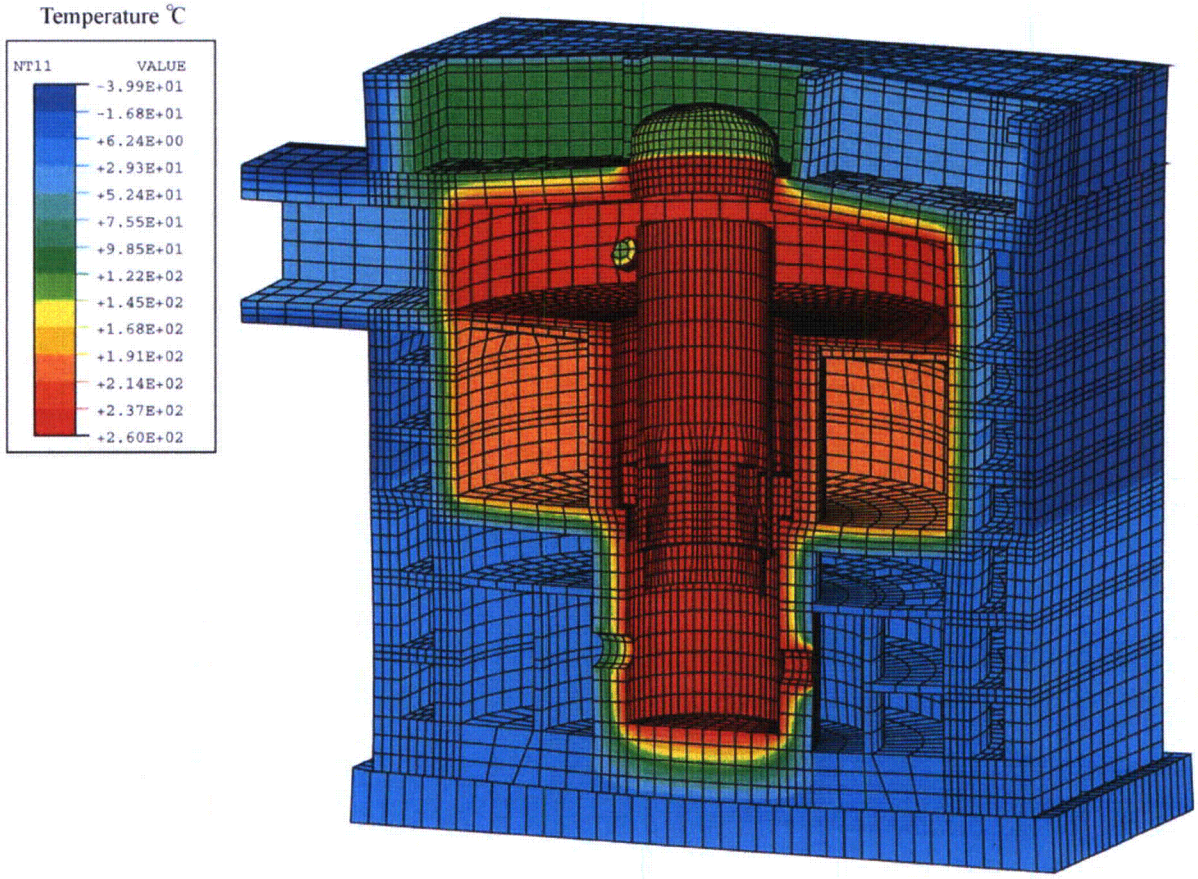

Figure 19B-1. Finite Element Model Showing Steady State Thermal Condition

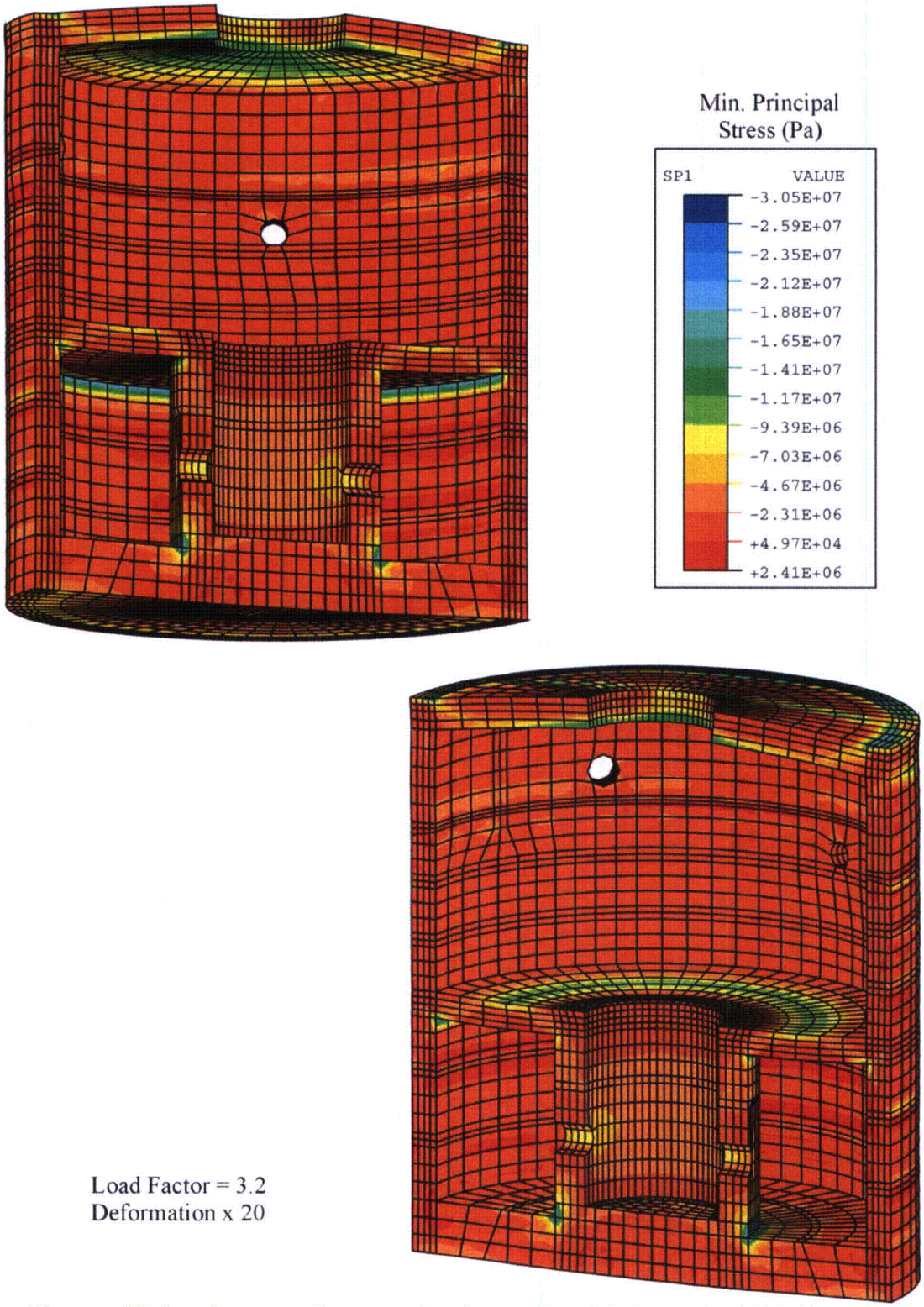

Figure 19B-2. Concrete Compressive Stress, Level C Analysis, 0.992 MPaG (144 psig) Pressure

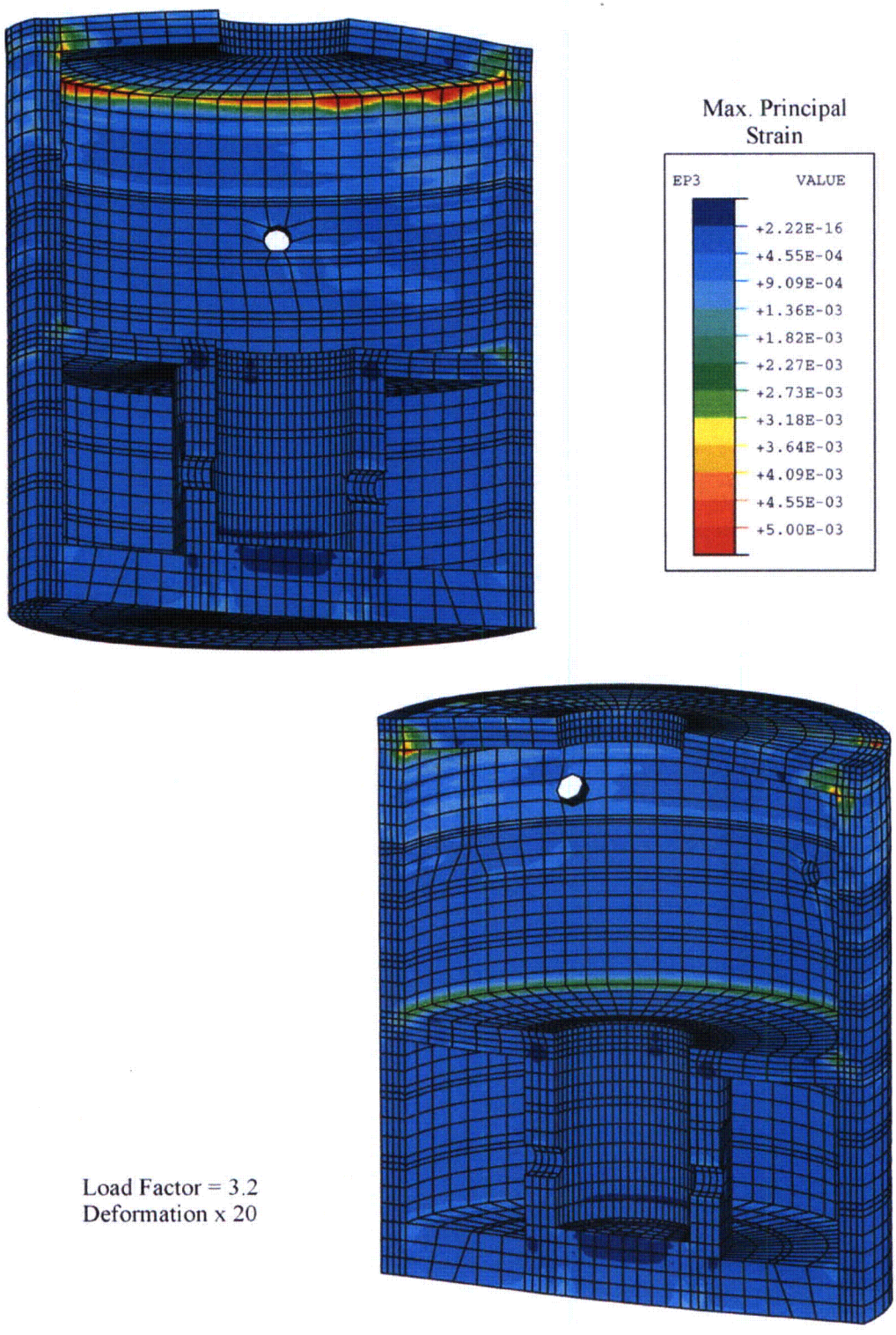

Figure 19B-3. Concrete Cracking Strain, Level C Analysis, 0.992 MPaG (144 psig) Pressure

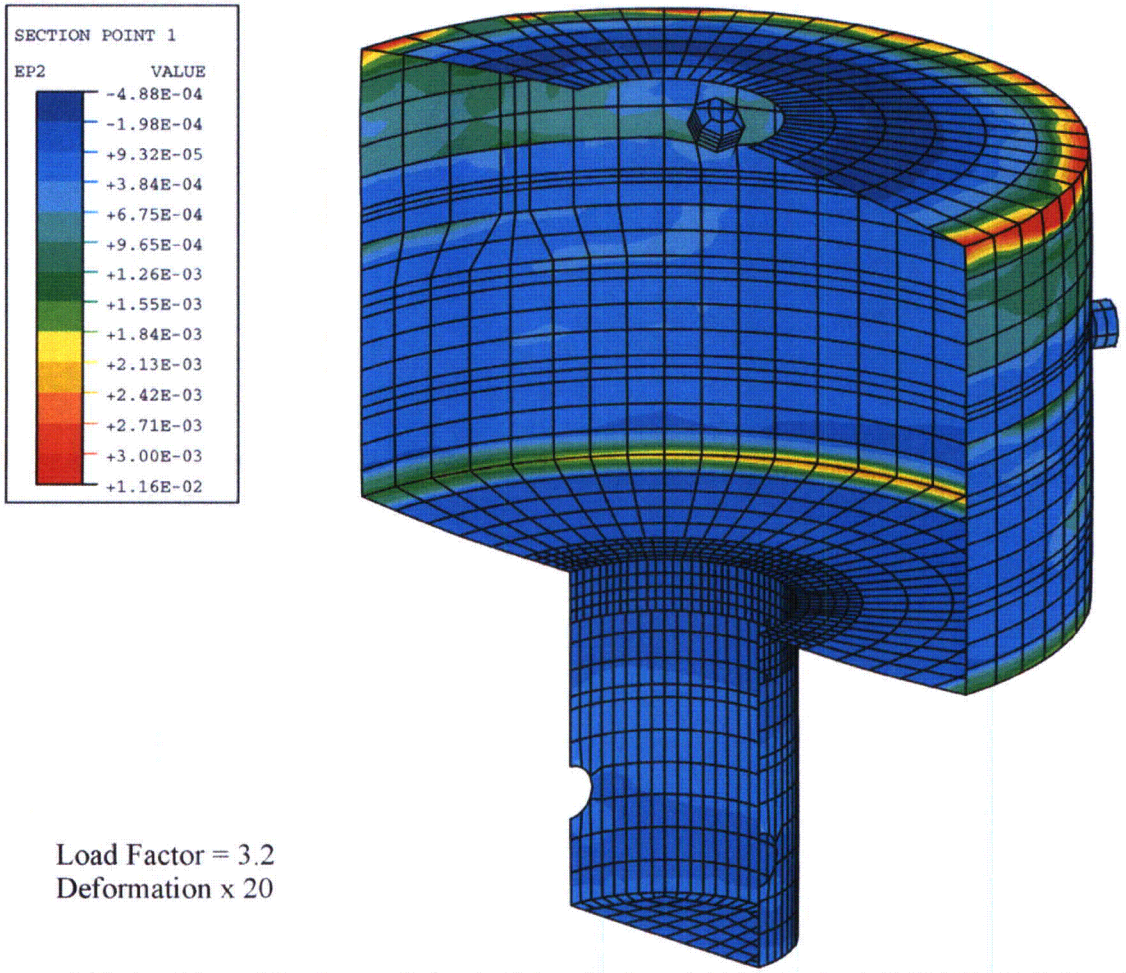

Figure 19B-4. Liner Maximum Principal Strain, Level C Analysis, 0.992 MPaG (144 psig) Pressure

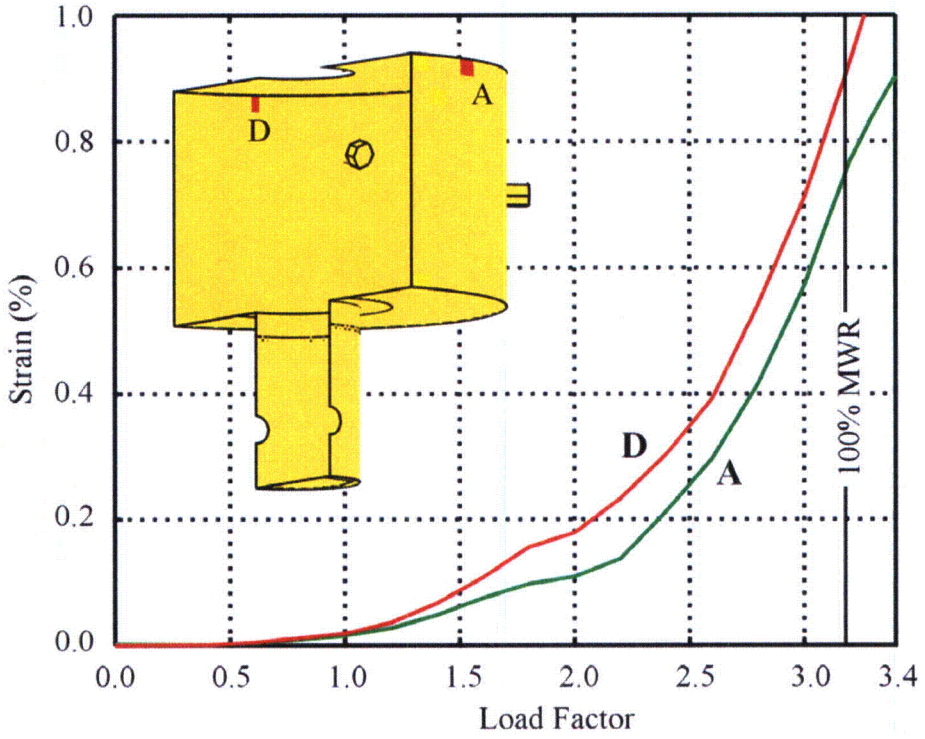

Figure 19B-5. Maximum Principal Strains in Liner Near Discontinuities, Level C Analysis

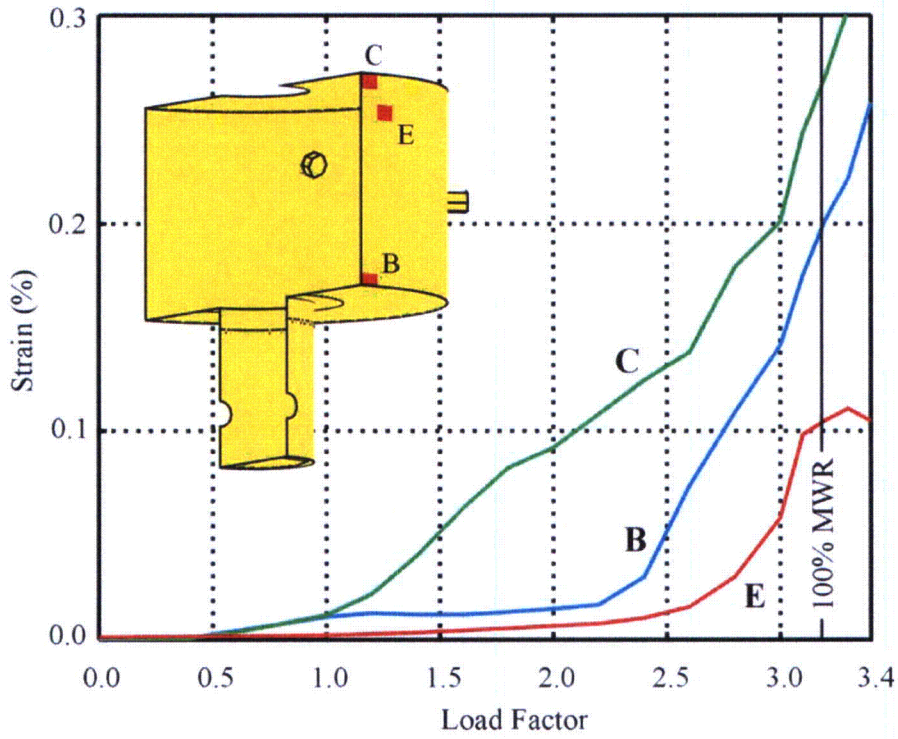

Figure 19B-6. Liner Membrane Strain at Representative Locations, Level C Analysis

Figure 19B-7. State of Liner at Top Slab Connection at 100% MWR Pressure (DELETED)

Figure 19B-8. Liner Membrane Strain at Top Slab Connection, Level C Analysis with Thermal Stress (DELETED)

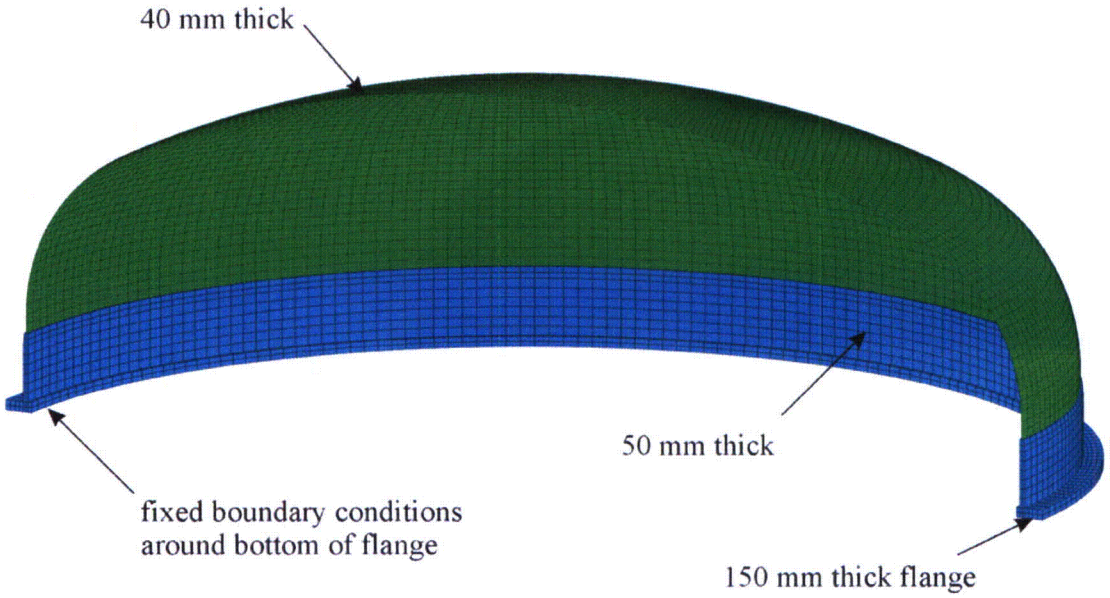

Figure 19B-7. Finite Element Model for Drywell Head Capacity Study

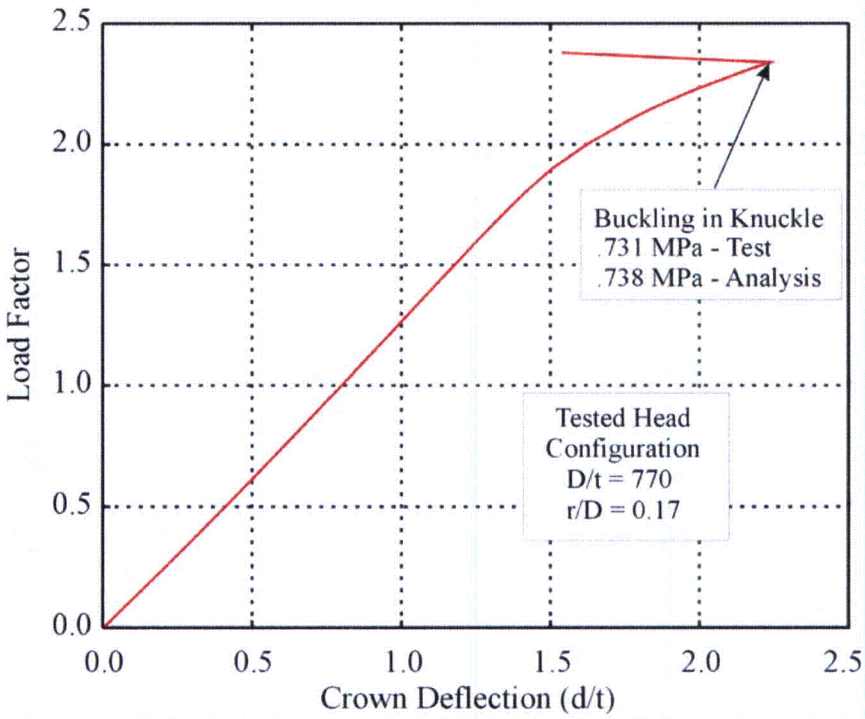

Figure 19B-8. Displacement at Crown in Buckling Test Analysis

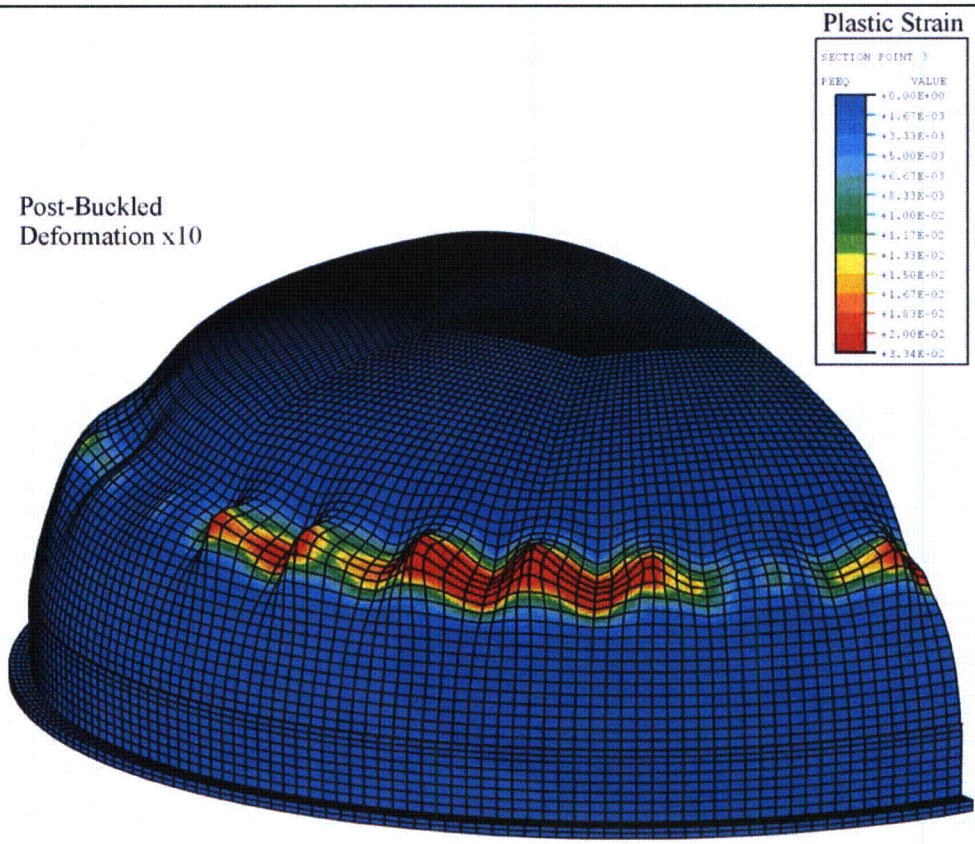

Figure 19B-9. Post Buckled Shape of Test Analysis Model

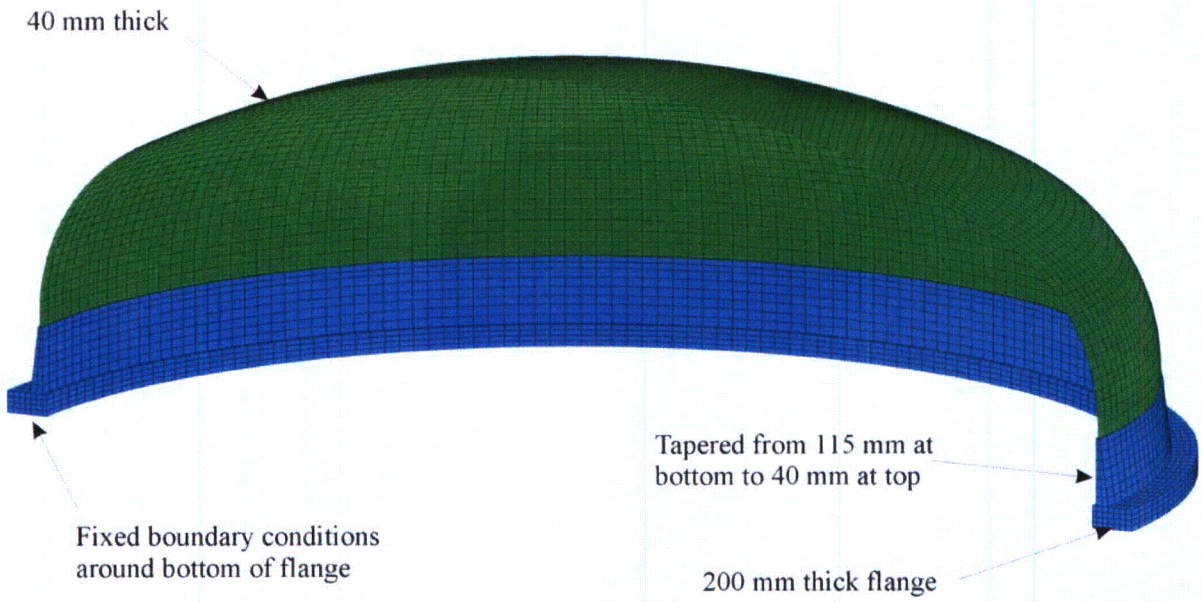

Figure 19B-10. Finite Element Model for Buckling Analysis of ESBWR Drywell Head

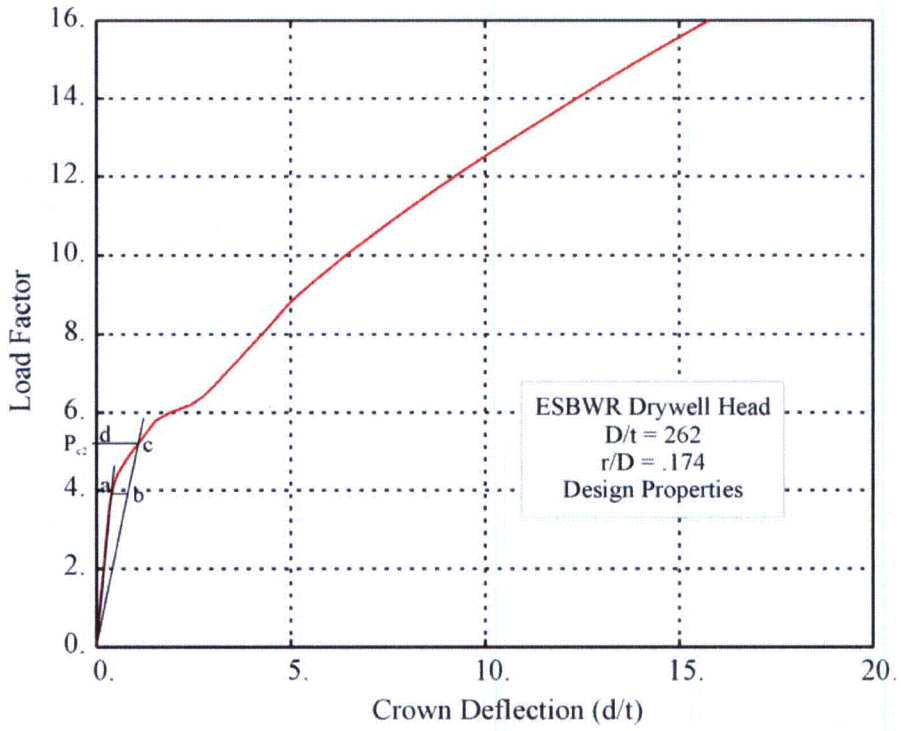

Figure 19B-11. Performance of ESBWR Drywell Head Under Internal Pressure at 260°C (500°F)

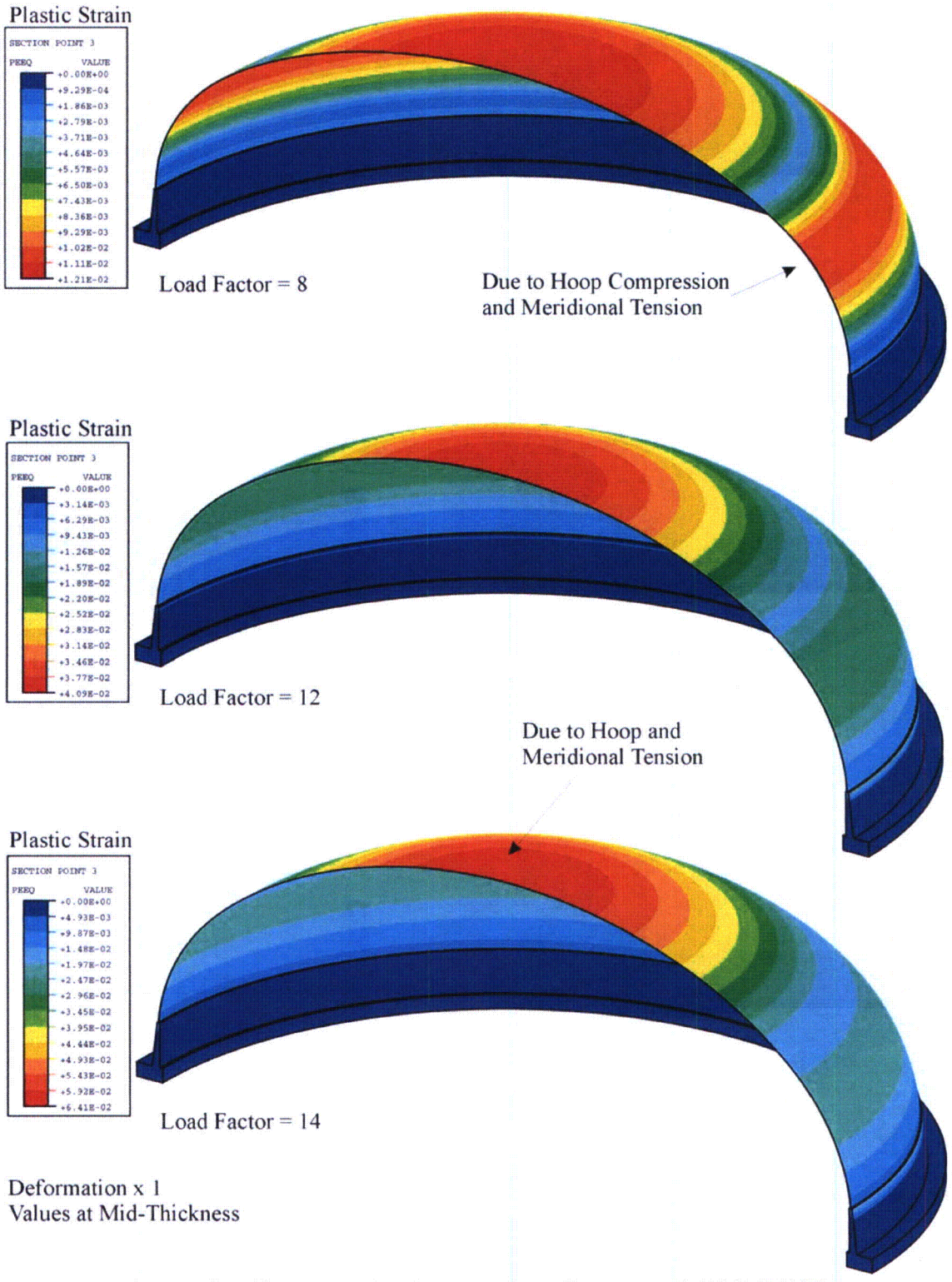

Figure 19B-12. Plastic Strains, Nominal Geometry, 260°C (500°F)

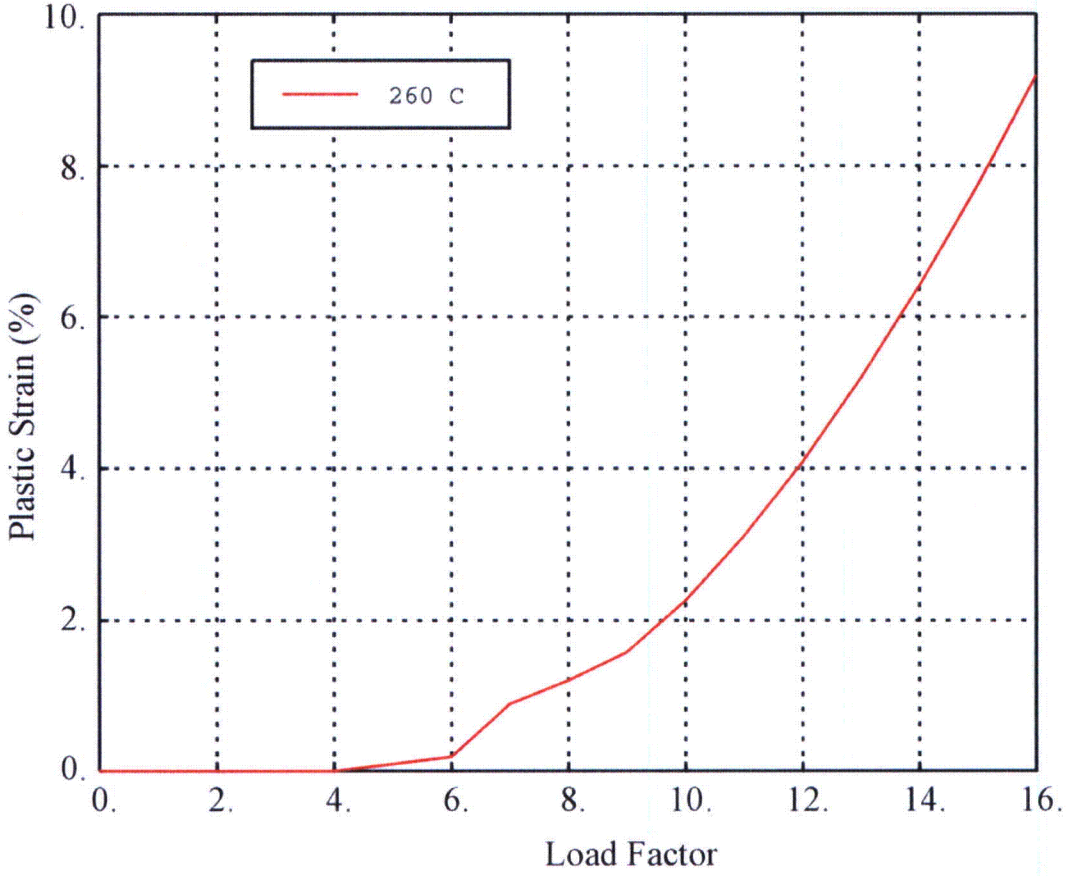

Figure 19B-13. Mid-Thickness Plastic Strain at Crown Under Increasing Pressure at 260°C (500°F)

19C. PROBABILISTIC ANALYSIS FOR CONTAINMENT PRESSURE FRAGILITY

19C.1 INTRODUCTION

This Appendix presents the probabilistic analyses and results for the fragility of the ESBWR primary containment system for over-pressurization. Fragility is defined as the cumulative probability of failure for increasing internal pressure. Here, failure of the containment is taken to mean a breach in the containment boundary, which can occur as a result of structural failure in the RCCV walls, liner tearing at discontinuities (such as anchorages, corner connections, or thickened plates at penetrations), rupture in the steel components of the penetrations or drywell head, or separation of the bolted flanges for the penetrations or drywell head. Analyses for the pressure capacity of these components requires different levels of modeling. A global, 3D finite element model is used to determine the pressure capacity of the RCCV structure assuming no leakage or failure in the steel penetration components. However, local detailed 3D models are used to determine the pressure limits associated with the steel components (drywell head and equipment hatch) using results from the global model as boundary conditions for the local models. The pressure units of MPaG used in this appendix are gauge pressures unless noted otherwise. Absolute pressure is designated as MPa.

For the current analyses, the thermal conditions corresponding to the 260°C (500°F) steady state accident conditions have been modified. For this accident condition, the temperature in the airspace under the drywell head is changed to be 260°C (500°F) corresponding to the atmosphere in the remainder of the drywell air space. Previously, the temperature on the inner surface of the drywell head was considered to be 43.3°C (110°F) with a transition to 260°C (500°F) across the barrel section of the drywell head in the top slab. In addition, the temperature of the water in the reactor well and in the equipment storage pool is changed from 43°C (110°F) to 100°C (212°F) due to heat flowing across the drywell head under these conditions. This new temperature condition affects the median pressure capacity determined for the RCCV global analysis because the global deformations and structural performance is dependent on the temperature in the upper water pools. The median pressure capacity for the drywell head determined from the local analysis is also affected because of the global deformations of the top slab and the higher temperatures on the drywell head, and also because of the updated bolt material and bolt preloads in Figure 3G.1-51.

However, the uncertainty in the calculations is not affected by this change in temperature conditions. The uncertainty is primarily associated with modeling methods, material properties, and failure criteria or structural limits used to establish the pressure capacity. The relative change in pressure capacity due to these uncertainties from the new median value will be very close to the relative change from the old median value that has previously been determined. Thus, it is not necessary to repeat the matrix of analyses with parameter variations to calculate the variance or standard deviation in the pressure capacity. New median pressure capacities are calculated for the RCCV global model and for the drywell head local model, and the new fragility is based on the previously calculated lognormal standard deviations.

Likewise, the new temperature conditions determined for the 260°C (500°F) steady state accident conditions do not affect the pressure capacity that has been previously calculated for the ambient condition or for the 538°C (1000°F) transient accident condition. The ambient case

does not consider any elevated temperatures, and the 538°C (1000°F) transient condition is based on a short term DCH temperature spike. Here, the temperatures under the drywell head and in the upper pools do not have time to react, and the previous assumptions for these temperatures are still valid. Thus, it is not necessary to repeat any of the analyses for pressure capacity at ambient conditions or at the 538°C (1000°F) transient conditions. The changes in conditions for the 260°C (500°F) steady state accident conditions also do not affect the temperature distributions already considered for the equipment hatch, and thus, new calculations to update the pressure capacities for the equipment hatch are not required.

19C.1.1 Analysis Methods

These analyses use the ANACAP-U concrete constitutive model (Reference 19C-1) coupled with the ABAQUS/Standard finite element computer program (Reference 19C-2). These analyses are based on detailed 3D finite element modeling, advanced material constitutive relations, and an assessment of uncertainties within a probabilistic framework. The uncertainties in the analysis results are associated with the finite element modeling, the material properties of the in-situ structure at the time of the accident, failure criteria or limit states used in establishing the pressure capacity, and the loading conditions that lead to pressurization of the containment. The uncertainties in the finite element modeling, such as mesh fidelity and constitutive relations, are discussed in Section 19C.1.5. The uncertainties in material properties and failure criteria are evaluated by first identifying those parameters that are likely to have a significant effect on the analysis results and then evaluating the effect of variations in these parameters using the 95% confidence value of the specific parameter while keeping all other parameters at the median values. The 95% confidence value is defined as V_m-1.645·β_v, where V_m is the median value of the property and β_v is the standard deviation for the distribution of the variation in that property. This represents a value such that there is 95% confidence that the actual value of that property will be larger than this value. In some cases, such as material property variations, additional analytical calculations are needed to evaluate the uncertainty. In other cases, such as variation in failure criteria, re-evaluation of an existing analysis result can be performed.

The failure pressure is characterized using a lognormal probability density function defined as

$$p_f(p) = \frac{1}{p\beta\sqrt{2\pi}} \exp\left[-\frac{1}{2}\left(\frac{\ln(p) - \mu}{\beta} \right)^2 \right] \qquad \text{(19C-1)}$$

where p is the failure pressure, μ is the mean value of the natural log of the failure pressure, and β is the standard deviation of the natural log of the failure pressure. Thus, the lognormal standard deviations for the various key parameters having uncertainty are determined using the equation

$$\beta_s^i = \frac{Ln(P_s^i / P_m)}{-1.645} \qquad \text{(19C-2)}$$

squares fit for the 2 parameters defining the lognormal PDF. The resulting curve fit is illustrated in Figure 19C-1.

Because the test data and analyses are all at ambient temperatures, the calculated β for modeling uncertainty is increased by 10% for the analyses associated with the 260°C (500°F) thermal conditions and by 20% for the analyses of the 538°C (1000°F) thermal conditions. Also, because the local modeling for the drywell head and equipment hatch take boundary conditions from the global model and perform additional analyses, the respective modeling uncertainties are increased by an additional variance of $\beta = 0.06$ which is typical for analyses of steel components. The values of lognormal standard deviations for modeling uncertainties are summarized in Table 19C-6.

19C.2 RCCV AND LINERS

19C.2.1 Model Description

A global 3D model is used to assess the ultimate capacity of the reinforced concrete components of the primary containment system due to over-pressurization under severe accident conditions. The modeling consists of a half-symmetric representation of the RCCV and the surrounding reactor building, including the basemat, the pedestal wall, the suppression pool floor slab, the upper drywell walls, the top slab, the upper pools structure and refueling floor, and the floors and walls of the reactor building, as illustrated in Figure 19C-2. This figure also illustrates the temperature distribution for the 260°C (500°F) steady state condition with deformations magnified by 10. It is noted that the temperature of the water in the reactor well and the equipment storage pool is now 100°C (212°F). The inner surface of the drywell head is 260°C (500°F) and the outer surface is 100°C (212°F). The global temperature plot is based on points near the outer surface for the plate elements representing the drywell head. The model is supported on an elastic layer of continuum elements representing the soil foundation. Solid (20-node continuum) elements with reduced Gaussian quadrature integration are used to model the reinforced concrete sections. The reinforcement bars are modeled as embedded, truss-like steel elements at the appropriate locations within the concrete elements. Membrane elements (plate elements without bending stiffness) are generally used to model the steel liners. These elements are attached to the nodes of the concrete elements for compatibility with the concrete deformations. This assumes that the liner anchorage system keeps the liners in contact with the concrete for this global modeling of the RCCV performance. Some plate bending elements are used for the thickened sections at connections. Representations for the large equipment hatches, personnel airlock penetrations, and the drywell head components are included using plate bending elements. Plate bending elements are also used to model the steel components of the internal structures, including the vent wall, diaphragm floor, reactor vessel shield wall, and the reactor pressure vessel support brackets, so that the stiffness and thermal induced stresses on the RCCV from these components are included in the modeling.

19C.2.2 Median Capacity Analysis

Figure 19C-3 plots the maximum principal strains, representative of cracking strains, in the RCCV at a drywell pressure of 4 times design pressure. This figure also shows the deformed shapes magnified by 10 and illustrates the structural response of the RCCV containment system. The contour limits in these plots are set to indicate distressed areas where cracking is

concentrated. The critical locations for the RCCV pressure capacity is at the connection of the RCCV upper drywell wall to the flat top slab, which is supported by the upper pool girders extending across the top slab. Cracking and distress is also evident in these upper pool main girders. Examination of the structural response relative to the failure criteria indicates that the pool girders will fail due to section shear capacity at a containment pressure of ~~1.913~~1.741 MPaG (~~277~~252 psig) or a load factor of ~~6.17~~5.61 times the design pressure. The critical location for liner tearing is at the connection of the RCCV wall to the top slab and, in particular, directly under the location of the upper pool girder on the top of the slab at the steam tunnel connection, as illustrated in Figure 19C-4. The calculated strain at this location is plotted versus internal pressure and evaluated against the failure criteria. Liner tearing is predicted to initiate at this top slab connection at a median pressure of ~~1.708~~1.643 MPaG (~~248~~238 psig) or a load factor of ~~5.51~~5.30 times the design pressure.

19C.2.3 Evaluation for Uncertainty

For the RCCV wall capacity, the important material property parameters are the concrete strength, which also affects the concrete modulus and tensile strength, and the yield strength of the reinforcement. The ultimate strength of the reinforcement also has uncertainty, but this is handled through the failure strain for the reinforcement. There is also uncertainty in the yield stress and ultimate strength of the liner material. However, for the global modeling, the evaluation for liner tearing is also handled through the failure strain limit for the liner. The liner yield stress is not considered an important parameter because the liner is "glued" to the concrete and thus deforms along with the concrete in a strain-controlled manner. Variations on the analysis for the 260°C (500°F) thermal condition are performed to establish the failure pressures under the 95% confidence values for these key parameters. Table 19C-7 summarizes the results of these studies for evaluation of the uncertainty. The table provides the failure pressures found and the calculated lognormal standard deviations for variation of the key parameters identified. The composite lognormal standard deviation including the modeling uncertainty is also shown in the table. As discussed previously, it is noted that the variance or uncertainty for the pressure capacity is not affected due to the new temperature conditions associated with the 260°C (500°F) steady state accident condition. The lognormal standard deviations for each area of uncertainty that have been previously computed relative to the previous median pressure capacities are used to assess the fragility with the current median pressure capacities.

19C.2.4 Variation with Temperature

To determine the variation of failure pressure with temperature for RCCV components, the global analyses using the median values of all parameters are performed for the other thermal conditions, namely normal operating (ambient) and the 538°C (1000°F) liner temperature under transient conditions. It is found that the RCCV response and mode of failure is the same as found in the 260°C (500°F) steady state thermal condition. The pressure capacity for the RCCV walls is again limited by shear failure of the upper pool girders spanning across the top slab. The calculated median pressure capacities for failure of the RCCV wall and liner tearing in the RCCV wall at the connection with the top slab for these thermal conditions are summarized in Table 19C-8.

19C.2.5 Summary

Table 19C-8 provides a summary of the pressure fragility for the capacity of the RCCV wall and for liner tearing at the connection of the RCCV wall to the top slab. This table provides the mean and standard deviations for the lognormal PDF function, along with the median value of pressure capacity and the 95% confidence value for the pressure capacity all for the variations in thermal conditions for an accident. The 95% confidence value is the pressure value such that there is a 95% confidence that the actual failure pressure will be higher. Figure 19C-5 illustrates the pressure fragility for the RCCV wall with temperature, and Figure 19C-6 plots the fragility with temperature for the RCCV liner tearing failure mode.

The pressure capacity of the RCCV structure is limited by tearing of the drywell liner on the RCCV wall at the connection to the top slab. The capacity of the actual RCCV wall is limited by shear failure of the main upper pool girders supporting the top slab. This failure in the supporting upper pool girder will lead to a subsequent rapid failure of the RCCV wall at the top slab connection. While the RCCV wall capacity has a higher median pressure capacity than liner tearing, it also has more uncertainty. This failure mode for the pressure capacity of the RCCV boundary does not change with temperature. The RCCV wall capacity shows a decrease of about ~~11~~20% from ambient conditions to elevated temperature conditions. This is due to the elevated water temperatures that develop in the upper pools under the steady state accident condition. ~~In addition, there is very little~~Likewise, the difference between the capacity at 260°C steady state conditions and the 538°C transient conditions is mainly because the upper pool girder controls this failure mode, and the performance of these upper pool girders is dependent on the temperature of the water in the pools. The resistance to liner tearing at the RCCV wall to top slab connections increases somewhat with temperature because of the effects of compressive stresses induced into the liner at elevated temperatures, which counteracts the tensile stress leading to tearing due to pressure. The liner material also has higher ductility at the upper range of the temperatures.

19C.3 DRYWELL HEAD

19C.3.1 Model Description

A detailed local model for the drywell head was constructed to evaluate the pressure fragilities for leakage from tearing in the steel components or from flange distortion and loss of seal. The drywell head model includes a section of the reinforced concrete top slab around the drywell head. Displacement boundary conditions, extracted from the global model, are imposed on the cut sections of the top slab in the local model. The boundary displacements enforce the deformation patterns from the global response of the containment system on the local model while capturing more refinement in the structural response of the drywell head components. A contact surface between the flanges is used to allow flange separation to develop. The closure bolts are modeled with beam elements with the appropriate length, cross-sectional area, and initial prestress. Figure 19C-7 illustrates the local modeling for the drywell head. This model for the drywell head was tested to insure that it can capture the buckling failure mode due to hoop compression in the knuckle region. The testing and analysis showing that the drywell head does not fail in this mode is discussed in Appendix 19B.

19C.3.2 Median Capacity Analysis

As in the global modeling, the evaluations for the median pressure capacity and the uncertainties in the analysis are performed for the 260°C (500°F) steady state thermal conditions. Figure 19C-8 illustrates the temperature distributions in the drywell head region along with the deformation patterns plotted at a load factor of 7 P_d with a magnification of 10. The top slab bulges upward due to the pressure in the drywell below. This forces the collar for the bottom flange to undergo bending deformations. Figure 19C-9 plots the accumulated plastic strain at a pressure of 2.17 MPaG (315 psig) or a load factor of 7 P_d for the steel components of the drywell head. The areas showing plastic deformation at this load are in the liners at the connections with the thickened shear plate and in the collar section at the connection with the top slab where the thickness taper ends. Evaluation of these locations against the steel tearing strain shows that tearing does not develop before bolt yielding and leakage past the seals in the flanges.

Figure 19C-10 illustrates the bending or prying deformation response in the bolted flanges and provides the bolt stresses versus pressure for the more critical bolt locations. For increasing internal pressure, the inside surface of the flanges begin to separate with increasing bearing stress around the toe of the flanges. Because of this prying action that produces substantial bearing stress and contact around the toe of the flanges, the pressure capacity is based on initiation of midsection yielding in the bolts. While the bolts can incur some additional plastic deformation before rupture, the median failure pressure is conservatively taken as that pressure causing first midsection yielding in the bolts. For the 260°C (500°F) steady state thermal condition, the median failure pressure for leakage at the bolted flange of the drywell head is ~~1.587~~1.426 MPaG (~~230~~207 psig) or ~~5.124~~.60 P_d.

19C.3.3 Evaluation for Uncertainty

A variation in the analyses using 95% confidence values for the yield stress of the steel material was performed to evaluate the variance due to uncertainty in this material property. Reevaluation of the median based analysis using the 95% confidence values of the strain limit for steel tearing and for bolt yield stress were performed to assess variance due to uncertainty in these parameters. Separate analyses were also performed using a 95% confidence value for the bolt prestress and another for the temperature distribution in the top head to assess the variance from uncertainty in these problem parameters. Table 19C-9 summarizes the results of these studies for evaluation of the uncertainty. The table provides the failure pressures found and the calculated lognormal standard deviations for variation of the parameters identified. The composite lognormal standard deviation including the modeling uncertainty is also shown in the table. For the drywell head penetration, the pressure capacity is controlled by leakage at the bolted flange from bolt yielding. In this case, the bolt prestress has little affect on the pressure capacity because of the stiffness of the flange and the prying action in the connection. Variation in the bolt yield has a direct affect on the pressure capacity. A reduced yield stress for the steel components has the effect of increasing the capacity from bolt yield because earlier yielding in the collar reduces the prying action on the bolts. However, bolt yielding still develops before tearing in the steel components so that the mode of failure does not change.

It is again noted that the variance or uncertainty for the pressure capacity of the drywell head remains the same as previously calculated from the matrix of parameter variations already considered.

19C.3.4 Variation with Temperature

The variation with temperature for the failure pressure causing leakage in the drywell head was evaluated using median based analyses for the ambient (normal operating) and 538°C (1000°F) transient thermal conditions. Thermal analyses, consistent with the global model analyses, are performed for the local drywell head model to establish the temperature distributions within the refined modeling. The loads due to increasing drywell pressure are then applied along with the boundary conditions from the global model at the corresponding load increments for the global analysis. Bolt yielding leading to leakage at the flange connection also limits the pressure capacity of the drywell head for these other temperature conditions. Both ambient and 538°C (1000°F) transient conditions provide somewhat higher capacities for pressure because the prying action at the flange is reduced for these cases due to global thermal deformation demands. ~~An extreme case with the inside of the drywell head held at 260°C (500°F) was also considered. This case also improved the pressure capacity due to bolt yielding. Here the elevated temperature on the inside of the head acts to keep the inner surface of the flanges together because the hot inner surface must expand. This thermal demand also resists the flange separation. Because there is very little effect on ultimate strength or ductility for this material up to 260°C (500°F), the mode of failure also does not change.~~

19C.3.5 Summary

Table 19C-10 provides a summary of the pressure fragility for the drywell head for the various thermal conditions. This table provides the mean and standard deviations for the lognormal PDF function, along with the median value of pressure capacity and the 95% confidence value for the pressure capacity. The 95% confidence value is the pressure value such that there is a 95% confidence that the actual failure pressure will be higher. Figure 19C-11 illustrates the pressure fragility for the drywell head with temperature.

19C.4 EQUIPMENT HATCHES

19C.4.1 Model Description

A detailed local model of a representative equipment hatch in the drywell was constructed to evaluate the pressure fragility for leakage from either tearing in the steel components or flange distortion and loss of seal. A hatch configuration in the upper drywell was chosen as the basis of the modeling. All equipment hatches have the same diameter, fabrication, section sizes, and closure configurations. The equipment hatch in the lower drywell differs only in that it penetrates the thicker pedestal wall. The thinner RCCV wall in the upper drywell will be more flexible and thus more critical for deformations leading to possible flange distortions or tearing in the steel components of the equipment hatch. The shear resistance along the barrel of the penetration is more critical for the thinner wall. The bolted flange connections perform similarly for the upper or lower drywell equipment hatches. The personnel airlock penetrations have a closure lid on the inside of the containment so that increasing pressure acts to keep this inner seal closed and the closure lid in compression. In addition, this configuration inhibits high temperatures during an accident from acting directly on the interior of the penetration. Thus, the equipment hatch in the upper drywell is used as the basis for this fragility analysis.

several differences between the test conditions for this Sandia 1:6 scale model and the configuration for the ESBWR equipment hatch penetrations. First, the Sandia 1:6 scale model did not have any internal support structures connected to the RCCV. Under internal pressure, the barrel section on this type of containment undergoes "ballooning" deformation, which develops large hoop strain at the locations of the penetrations. In the ESBWR, the drywell equipment hatch is located just above the diaphragm floor connection with the RCCV wall, and the RCCV is integral with the reactor building floors connecting to the exterior of the RCCV. This internal and external support for the ESBWR configuration restricts the radial deformation and hoop strains near the equipment hatch. Secondly, the Sandia 1:6 scale model employed stud type anchorages for the liner, while the ESBWR design uses continuous vertical T-beams for anchoring the liner to the RCCV wall. The continuous vertical anchorages along the edges of the thickened plates at the penetrations provide more support for this connection than the stud type anchorages. Finally, these analyses also consider thermal loads due to elevated temperatures, whereas the Sandia 1:6 scale tests were conducted at uniform ambient temperatures. The thermal loads cause compressive membrane stress in the liner that counteracts the tension stress under the pressure loads. Thus, while the level of tension strain needed in the analysis to cause failure may be similar to that determined from the Sandia 1:6 scale model testing, the pressure levels required to develop that strain in the ESBWR analyses is larger as a relative factor on the design pressure.

19C.5 PRESSURE FRAGILITY SUMMARY

The fragility of the ESBWR primary containment system to over-pressurization under accident conditions is summarized in Table 19C-13. This table provides the median value and a 95% confidence value for the failure pressures causing the various failure modes leading to a breach in the containment boundary. The failure pressures are provided in terms of a factor on the design pressure of 0.31 MPaG (45 psig) and as the actual gauge pressure (MPaG). Additional failure mechanisms for tearing of the liner, either at the equipment hatch penetration or drywell head connections, and tearing of the steel components for the equipment hatch and drywell head were also considered but were not controlling. Figure 19C-16 plots the fragility for the various failure modes for the 260°C (500°F) steady state thermal condition. The median pressure capacity for this condition is limited by leakage at the drywell head flange which is caused by bolt yielding. The subsequent failure modes, in order of increasing median failure pressure limits, are: 1) tearing of the liner at the connection of the RCCV wall to the top slab, 2) failure of the RCCV wall at the connection with the top slab due to shear failure of the upper pool girders supporting the top slab, and 3) leakage at the bolted flange connection of the equipment hatch type penetrations due to flange separation~~, and 3) failure of the RCCV wall at the connection with the top slab due to shear failure of the upper pool girders supporting the top slab.~~ Under normal operating (ambient) thermal conditions, the pressure capacity is limited by tearing of the liner at the RCCV wall connection with the top slab. For the 538°C (1000°F) transient thermal condition, the pressure capacity is limited by leakage at the bolted flange connection in the equipment hatch. In this scenario, the inside of the equipment hatch penetration is exposed to the extreme temperatures considered, and capacity is significantly reduced by thermal induced stress at this bolted connection. ~~Note that the drywell head is protected from these extreme temperatures because of insulation around the RPV and restricted flow paths from the drywell~~

~~space into the area beneath the drywell head. The pool of water on top of the drywell head also keeps the flanges and closure bolts at moderate temperatures.~~

19C.6 REFERENCES

19C-1. ANACAP-U, Version 2.5, Theory Manual, ANA-QA-145, ANATECH Corp., San Diego, CA, 1998.

19C-2. ABAQUS/Standard, Version 5.8, Hibbitt, Karlssen, and Sorensen, Inc., Pawtucket, RI, 1998.

19C-3. Rodabaugh, E. C., and Desai, K. D., "Realistic Seismic Design Margins of Pumps, Valves, and Piping," NUREG/CR-2137, USNRC, Washington, DC, June 1981.

19C-4. Chu, T. Y., Pilch, M. M., et. al., "Lower Head Failure Experiments and Analyses," NUREG/CR-5582, USNRC, Washington, DC, February 1999.

19C-5. Brister, P. M., "Code Design Criteria in the USA, Evaluation of Strength Properties," Proceedings of the 3rd International Conference on Pressure Vessel Technology, Tokyo, Japan, April 18-22, 1977.

19C-6. Interim Guidelines Advisory No. 2, Chapter 8. Metallurgy and Welding, SAC 99-01, Applied Technology Council, University of California, Berkely, CA, 1994.

19C-7. Luecke, W. E., et. al., "Mechanical Properties of Structural Steels," NIST NCSTARR 1-3D, Federal Building and Fire Safety Investigation of the World Trade Center Disaster, National Institute of Standards and Technology, Washington, DC, September 2005.

19C-8. Bournonville, M., Dahnke, J., and Darwin, D., "Statistical Analysis of the Mechanical Properties and Weight of Reinforcing Bars," Report SL 04-1, Structural Engineering and Engineering Mechanics, University of Kansas, December 2004.

19C-9. Brinkman, C. R., Sikka, V. K., and King, R. T., "Mechanical Properties of Liquid-Metal Fast Breeder Reactor Primary Piping Materials," Nuclear Technology, Vol. 33, pages 77-95, April 1977.

19C-10. ITER Material Properties Handbook for Series 300 Stainless Steel, Document No. S 74 RE 1.

19C-11. Freskakis, G. H., "State-of-the-Art Report on High Temperature Concrete Design," Burns and Roe, Inc., Oradell, NJ, for U. S. Department of Energy, DOE/CH/94000-1, November 1985.

19C-12. "High Performance Steels for Bridges: HPS 70W," International Steel Group, Inc., Technical Specification Overview.

19C-13. James, R. J., Zhang, L., Rashid, Y. R., "Impact of High Velocity Objects into Concrete Structures – Methodology and Application," Proceedings of ASME International Mechanical Engineering Congress and Exposition, Washington, D. C., November, 2003.

Table 19C-1
Summary of Thermal Material Properties

Material	Weight Density (MN/m^3)	Specific Heat (J/kg-K)	Conductivity (W/m-K)
Concrete	0.0235	878.64	1.6
Carbon Steel Liner	0.0770	460.24	53.5
Stainless Steel Liner	0.0770	493.71	16.3
Structural Steel	0.0770	460.24	53.5

Table 19C-2
Summary of Elastic Mechanical Properties for Steels

	Ambient Conditions		260°C Conditions		538°C Conditions	
	Median	**95 %**	**Median**	**95 %**	**Median**	**95 %**
Carbon Steel						
Modulus (GPa)	203.4	200.0	185.1	182.0	122.1	120.0
Poisson's Ratio	0.289	0.289	0.295	0.295	0.304	0.304
Stainless Steel						
Modulus (GPa)	200.0	198.6	180.0	178.8	158.0	156.9
Poisson's Ratio	0.295	0.295	0.311	0.311	0.331	0.331
Bolting Material						
Modulus (GPa)	204.77	201.33	190.44	184.09	161.77	148.24
Poisson's Ratio	0.289	0.289	0.295	0.295	0.304	0.304

Table 19C-3
Summary of Plastic Mechanical Properties for Steels

	Ambient Conditions		260°C Conditions		538°C Conditions	
	Median	**95 %**	**Median**	**95 %**	**Median**	**95 %**
SA516 Grade 70						
Yield Stress (MPa)	335.3	295.3	301.8	265.3	261.5	211.2
Tensile Strength (MPa)	531.3	491.9	488.8	460.2	438.3	350.2
Elongation (%)	20.3	17.0	20.5	16.4	33.7	24.0
A572 Grade 50						
Yield Stress (MPa)	397.2	344.8	317.8	254.1	226.4	157.0
Tensile Strength (MPa)	521.4	451.0	516.2	438.8	318.0	233.6
Elongation (%)	22.5	18.0	25.0	20.0	30.0	24.0
A36						
Yield Stress (MPa)	339.3	287.1	271.4	214.0	193.4	130.8
Tensile Strength (MPa)	472.4	416.8	467.7	406.5	288.2	221.5
Elongation (%)	35.4	26.0	40.3	30.0	45.3	34.0
A709 HPS 70W						
Yield Stress (MPa)	554.8	495.9	443.9	357.0	316.3	226.1
Tensile Strength (MPa)	652.1	629.0	645.6	560.4	397.8	306.9
Elongation (%)	23.8	19.0	26.3	21.0	28.8	23.0
A615 Grade 60 Rebar						
Yield Stress (MPa)	473.1	437.9	378.5	315.3	269.7	199.7
Tensile Strength (MPa)	724.1	669.0	716.9	596.0	441.7	326.5
Elongation (%)	12.5	8.6	13.0	9.0	14.0	10.0
SA240 SS 304L						
0.2% Yield Stress (MPa)	200.0	179.4	137.5	106.6	108.3	78.2
Tensile Strength (MPa)	487.5	453.2	376.7	344.4	337.5	303.2
Elongation (%)	57.5	48.6	39.2	29.6	35.8	26.2
SA437 Grade B4B Bolting						
Yield Stress (MPa)	769.5	724.1	666.5	616.6	516.8	462.3
Tensile Strength (MPa)	1045.4	1000.0	901.5	851.5	692.9	638.5
Elongation (%)	15.5	13.0	16.6	14.1	17.6	15.2

Table 19C-7
Summary of Uncertainty Evaluations for RCCV Pressure Capacity

Parameter	Type	RCCV Failure due to Section Shear Failure in Upper Pool Girders		Liner Tear at Connection of RCCV Wall to Top Slab	
		Pressure MPaG (LF on P_d)	β	Pressure MPaG (LF on P_d)	β
Median Failure Pressure	Median Values	1.741 (5.61)	--	1.643 (5.30)	--
Concrete Strength (MPa)	Material Property	1.624 (5.24)	0.0993	1.590 (5.13)	0.0434
Rebar Yield Stress (MPa)	Material Property	1.907 (6.15)	0.002	1.640 (5.29)	0.0248
Section Shear Strain Limit (%)	Failure Criterion	1.615 (5.21)	0.1028	N/A	--
Rebar Rupture Strain (%)	Failure Criterion	N/A	--	N/A	--
Liner Tearing Strain (%)	Failure Criterion	N/A	--	1.587 (5.12)	0.0446
Modeling Uncertainty (Section 4.6)	Modeling Methods	--	0.1355	--	0.1355
Composite Lognormal Standard Deviation	Composite	--	0.1970	--	0.1512

Note:
The median pressure capacities are updated to reflect the current analyses, but the β values, previously computed relative to the previous median pressure capacities, do not change.

Table 19C-8
Summary of Pressure Fragility for RCCV and Liner

Failure Mode and Thermal Condition	PDF Lognormal Distribution		Failure Pressure, MPaG (Load Factor on P_d)	
	μ	β	Median Value	95% Value
RCCV Capacity due to Shear Failure in Pool Main Girder				
260°C Steady State	1.705	0.1970	1.741 (5.61)	1.234 (3.98)
Ambient Steady State	1.911	0.1887	2.133 (6.88)	1.536 (4.95)
538°C Transient	1.807	0.2056	1.928 (6.22)	1.346 (4.34)
Liner Tear at RCCV Wall Connection with Top Slab				
260°C Steady State	1.656	0.1512	1.643 (5.30)	1.267 (4.09)
Ambient Steady State	1.648	0.1403	1.628 (5.25)	1.280 (4.13)
538°C Transient	1.752	0.1623	1.810 (5.84)	1.368 (4.41)

Table 19C-9
Summary of Uncertainty Evaluations for Drywell Head Pressure Capacity

Parameter	Type	Leakage Due to Bolt Yielding		Leakage Due to Steel Tearing	
		Pressure MPaG (LF on P_d)	β	Pressure MPaG (LF on P_d)	β
Median Failure Pressure	Median Values	1.426 (4.60)	--	2.291 (7.39)	--
Steel Yield Stress (MPa)	Material Property	1.652 (5.33)	-0.0244	2.114 (6.82)	-0.0292
Steel Rupture Strain (%)	Failure Criterion	N/A	--	1.705 (5.50)	0.1016
Drywell Head Temperature	Loading Condition	1.587 (5.12)	0.00	--	--
Bolt Prestress (MPa)	Loading Condition	1.587 (5.12)	0.00	1.975 (6.37)	0.0123
Bolt Yield Stress (MPa)	Failure Criterion	1.507 (4.86)	0.0317		--
Modeling Uncertainty (Section 4.6)	Modeling Methods	--	0.1482		0.1482
Composite Lognormal Standard Deviation	Composite	--	0.1535		0.1824

Note:
The median pressure capacities are updated to reflect the current analyses, but the β values, previously computed relative to the previous median pressure capacities, do not change.

Table 19C-10
Summary of Pressure Fragility for Drywell Head

Failure Mode and Thermal Condition	PDF Lognormal Distribution		Failure Pressure, MPaG (Load Factor on P_d)	
	μ	β	Median Value	95% Value
Leakage Due to Bolt Yielding				
260°C Steady State	1.514	0.1535	1.426 (4.60)	1.095 (3.53)
Ambient Steady State	1.846	0.1428	1.983 (6.40)	1.552 (5.01)
538°C Transient	1.760	0.1645	1.826 (5.89)	1.374 (4.43)

Table 19C-13
Summary of ESBWR Fragility for Over-Pressurization

Failure Mode	Failure Pressure Factor on P_d Followed by Gauge Pressure (MPaG)					
	Ambient Conditions		260°C (500°F) Steady State		538°C (1000°F) Transient	
	Median	95%HC	Median	95%HC	Median	95%HC
DW Head Leakage due to Bolt Yielding	6.40 1.983	5.01 1.552	4.60 1.426	3.53 1.095	5.89 1.826	4.43 1.374
Liner Tearing RCCV Wall at Top Slab	5.25 1.628	4.13 1.280	5.30 1.643	4.09 1.267	5.84 1.810	4.41 1.368
EQ Hatch Leakage - Flange Separation	6.49 2.012	5.07 1.573	6.07 1.882	4.65 1.443	3.81 1.181	2.86 0.888
RCCV Wall at Top Slab Connection	6.88 2.133	4.95 1.536	5.61 1.741	3.98 1.234	6.22 1.928	4.34 1.346

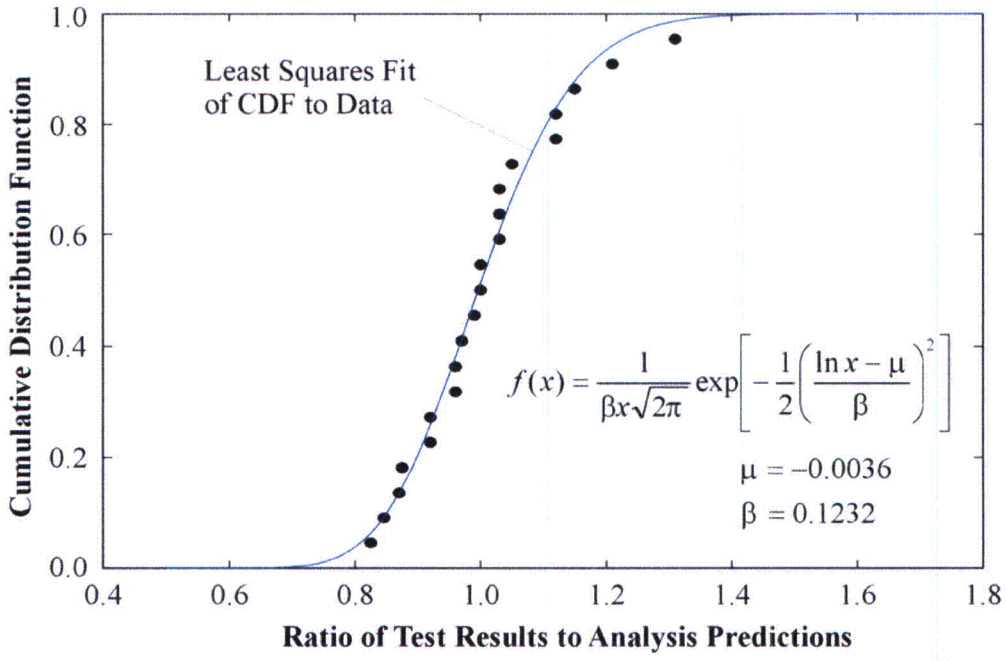

Figure 19C-1. Calculation of Variance due to Modeling Uncertainty

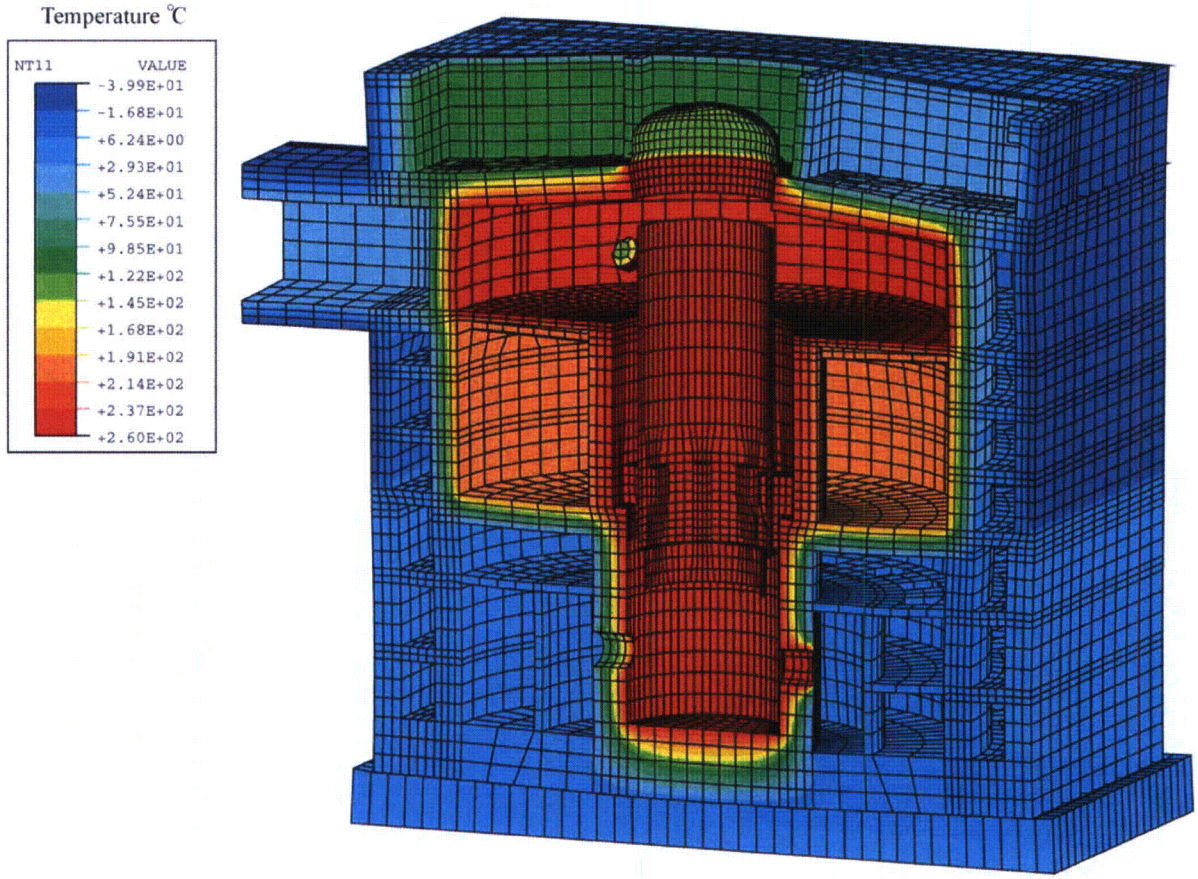

Figure 19C-2. Finite Element Model Showing the 260°C (500°F) Steady State Thermal Condition

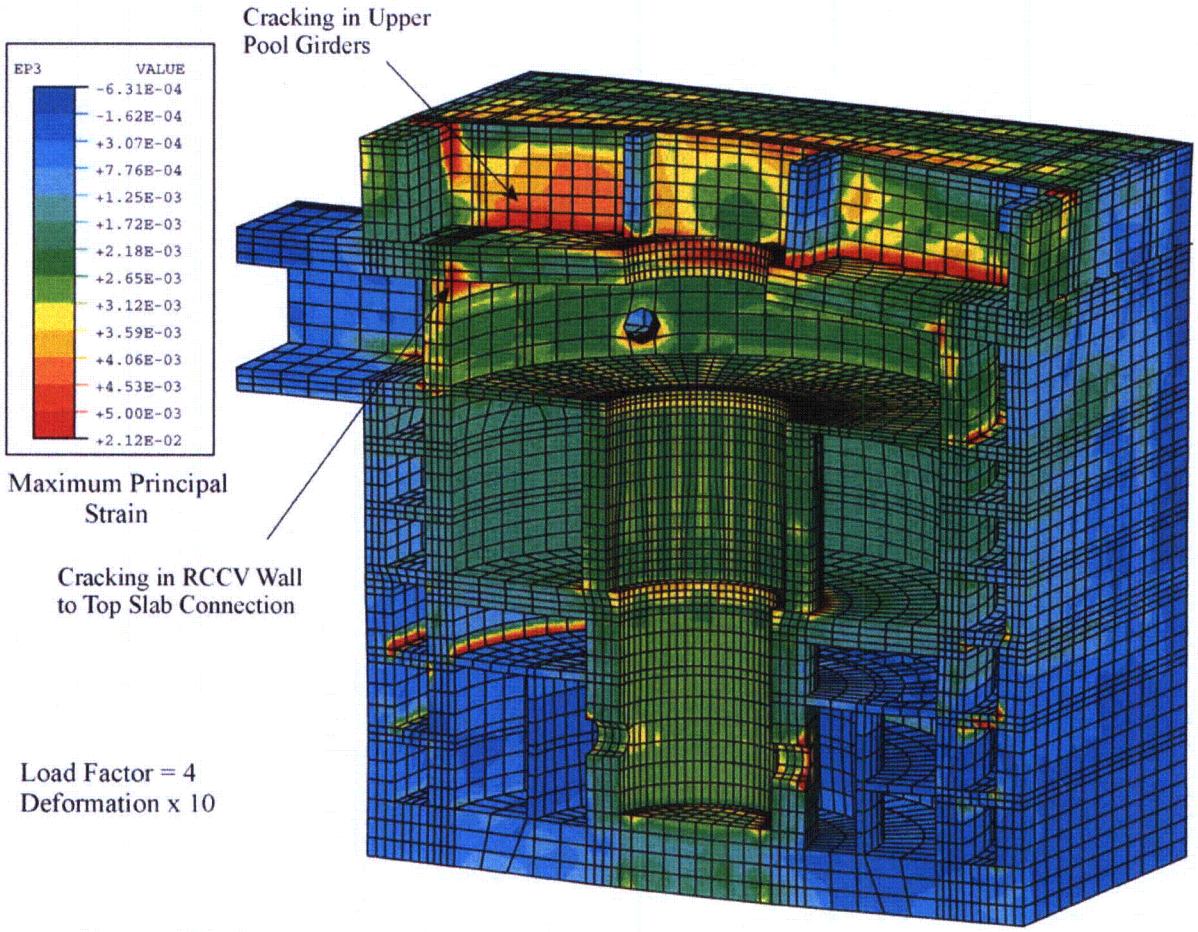

Figure 19C-3. Structural Response of RCCV at 1.24 MPaG (180 psig) Pressure

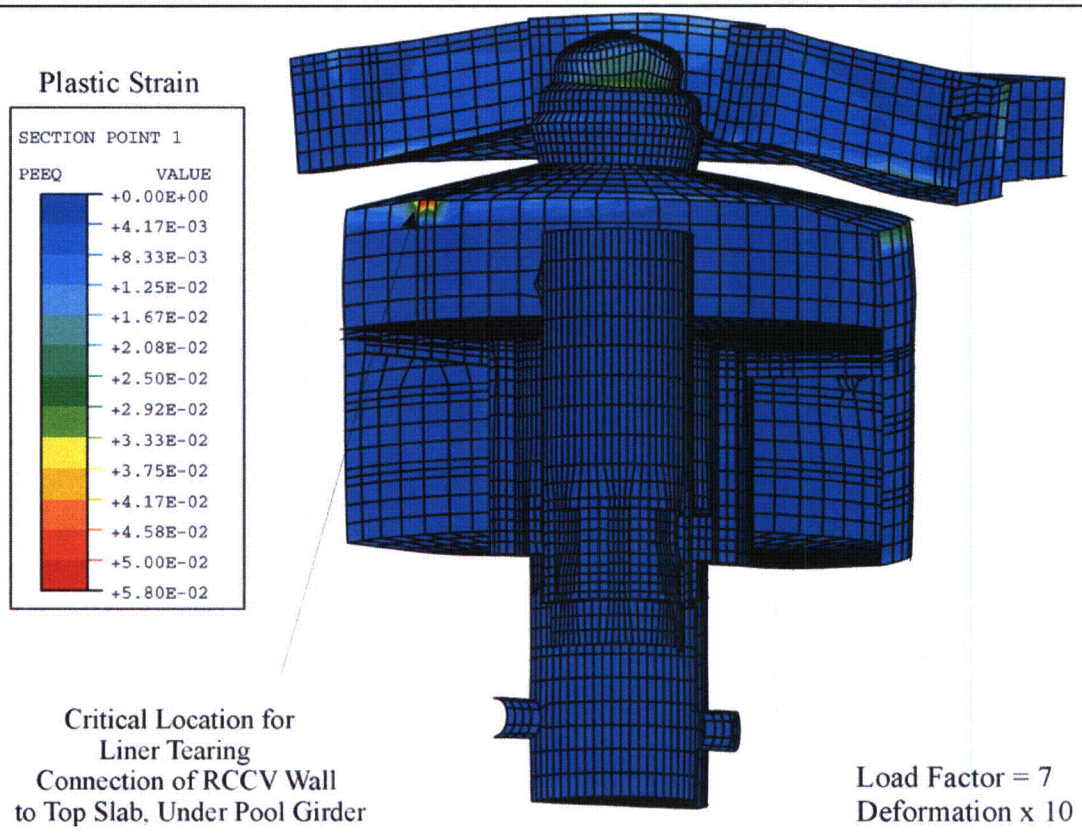

Figure 19C-4. Critical Location for Liner Tearing in RCCV

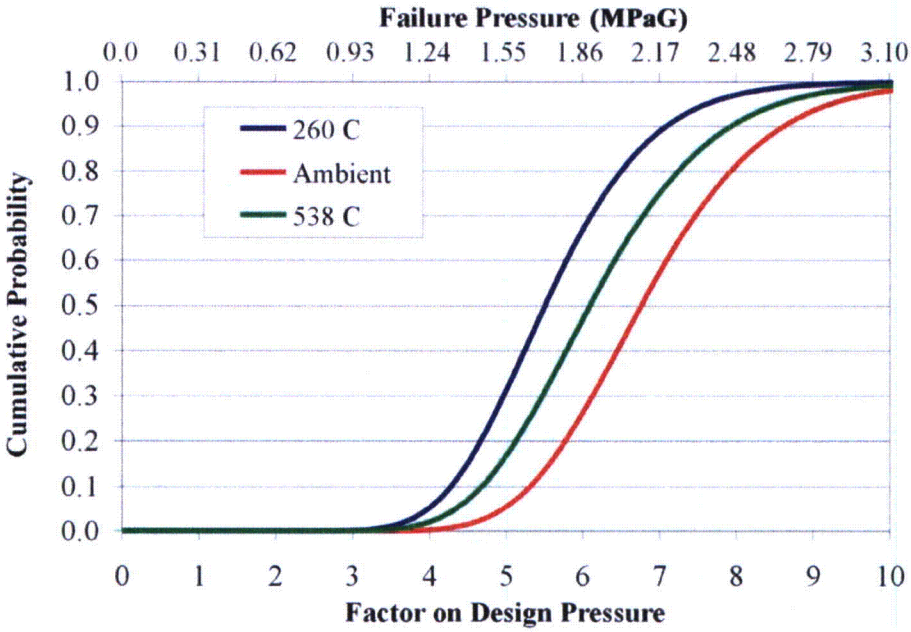

Figure 19C-5. Pressure Fragility for RCCV Wall Capacity with Temperature

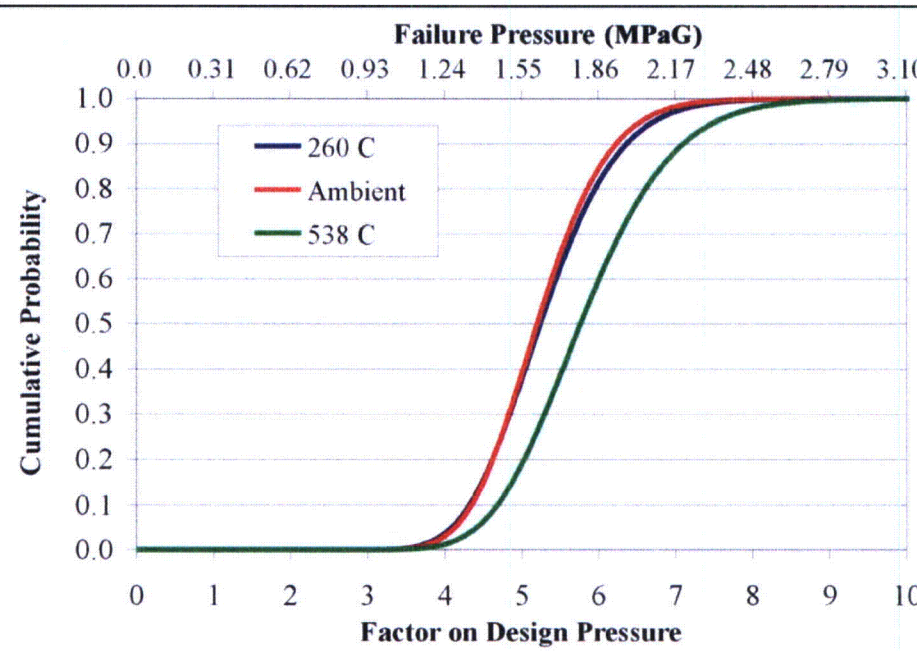

Figure 19C-6. Pressure Fragility for RCCV Liner Tearing with Temperature

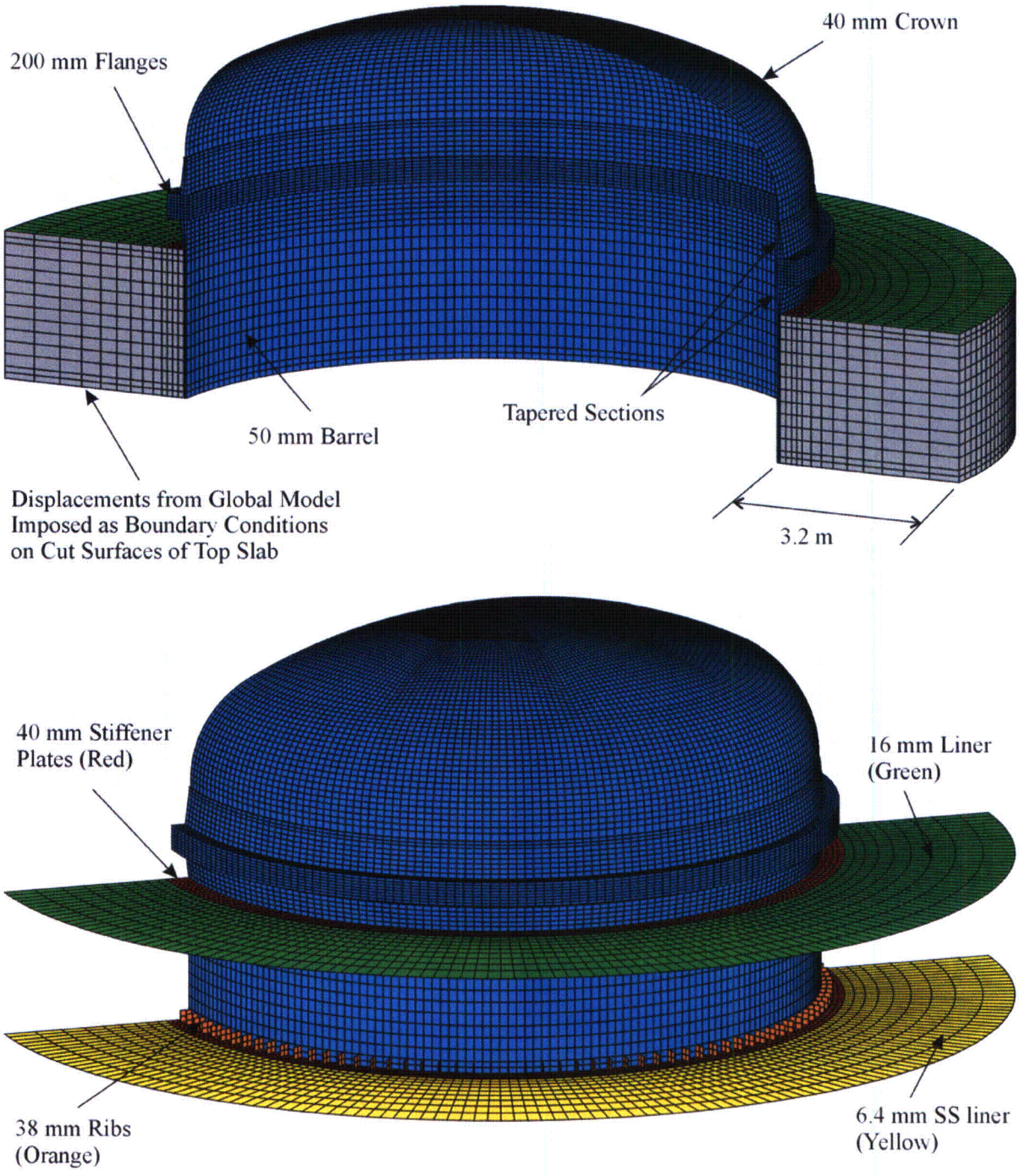

Figure 19C-7. Local Finite Element Model for Drywell Head

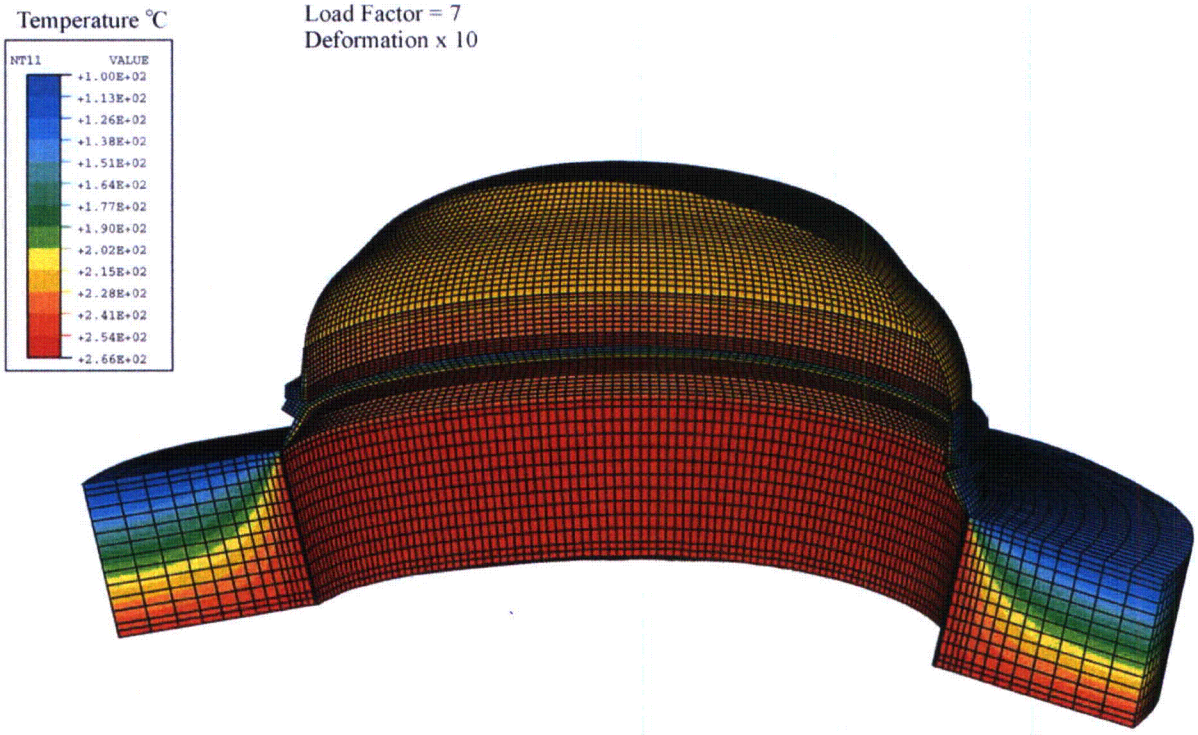

Figure 19C-8. Thermal Contours and Deformation for 260°C (500°F) Thermal Condition

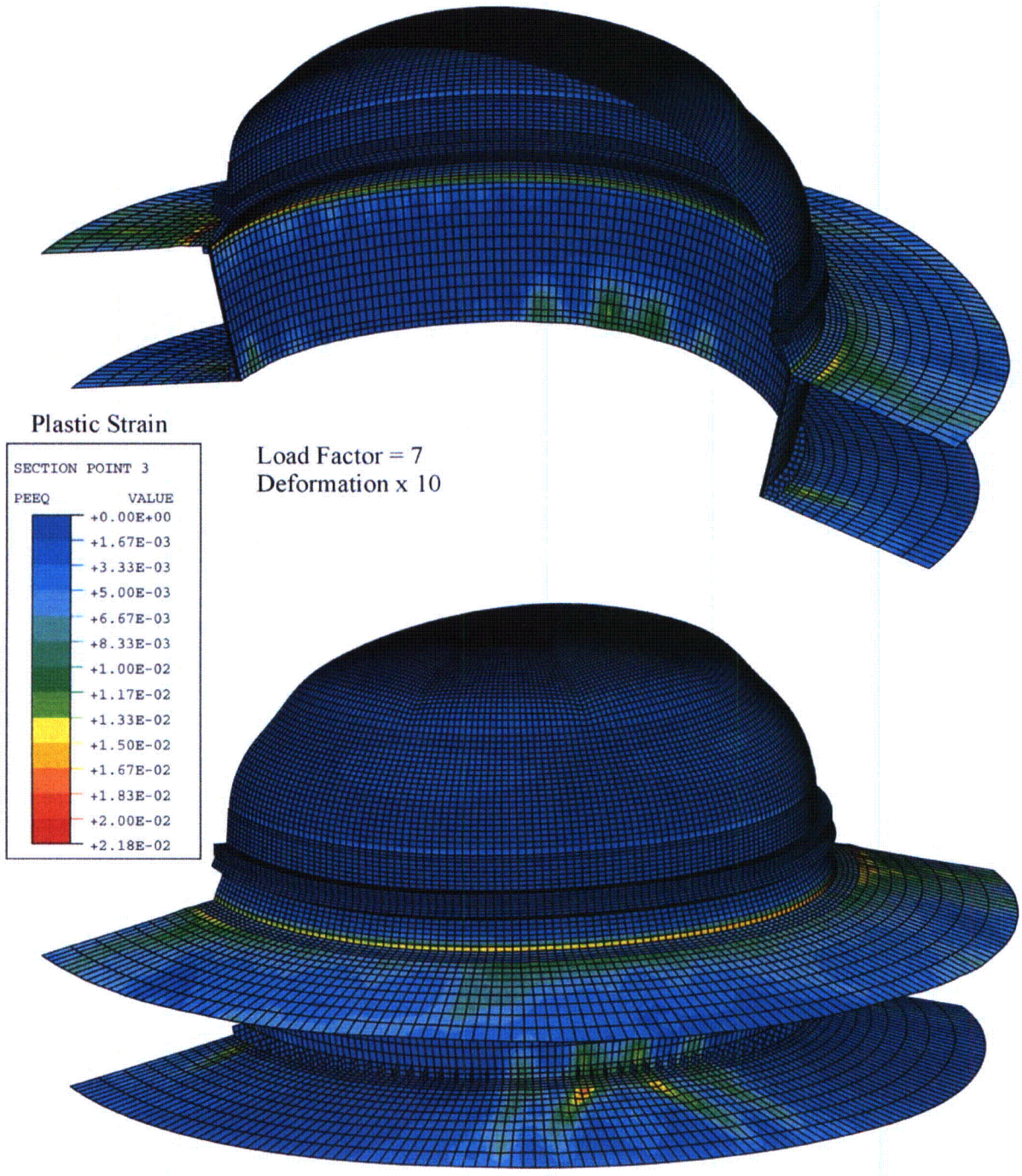

Figure 19C-9. Equivalent Plastic Strains in Steel Components at 2.17 MPaG (315 psig)

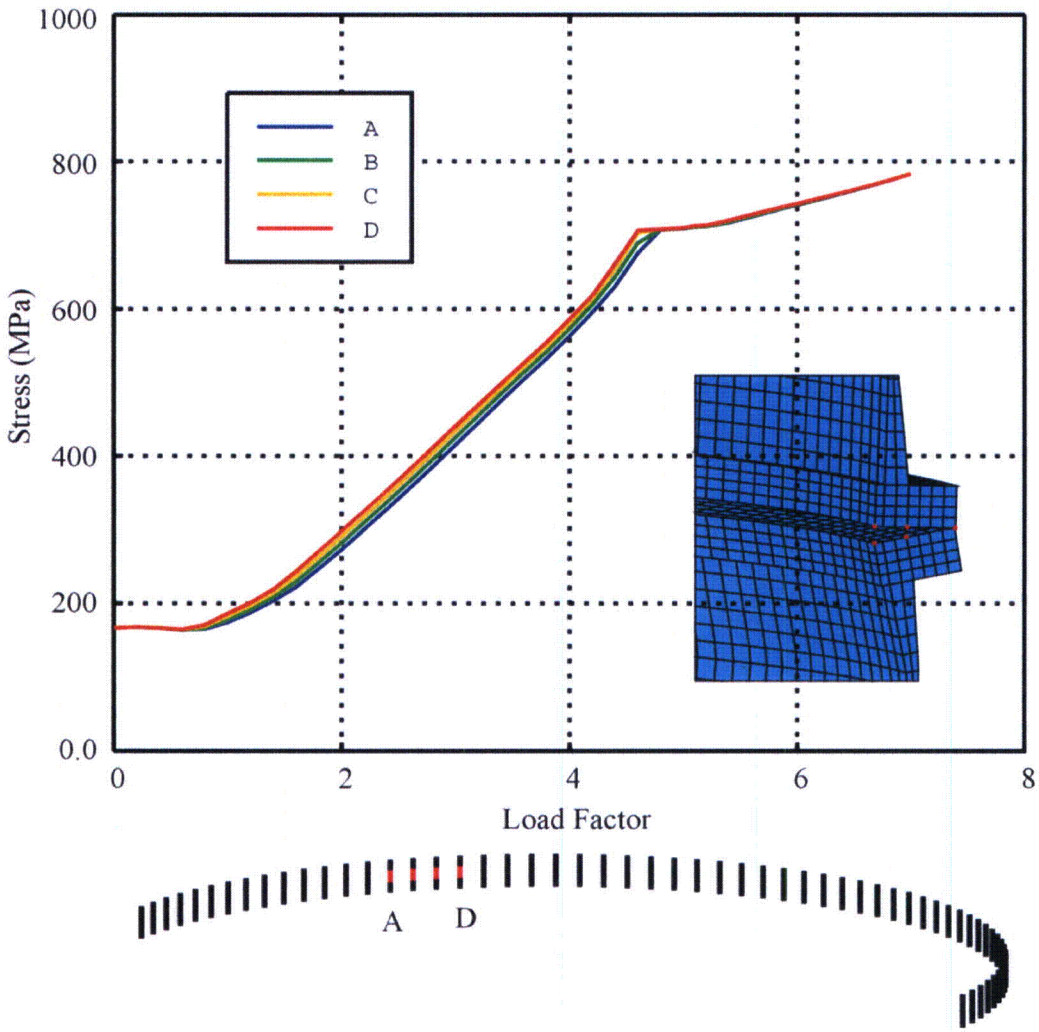

Figure 19C-10. Bolt Stresses in Drywell Head for 260°C (500°F) Thermal Condition

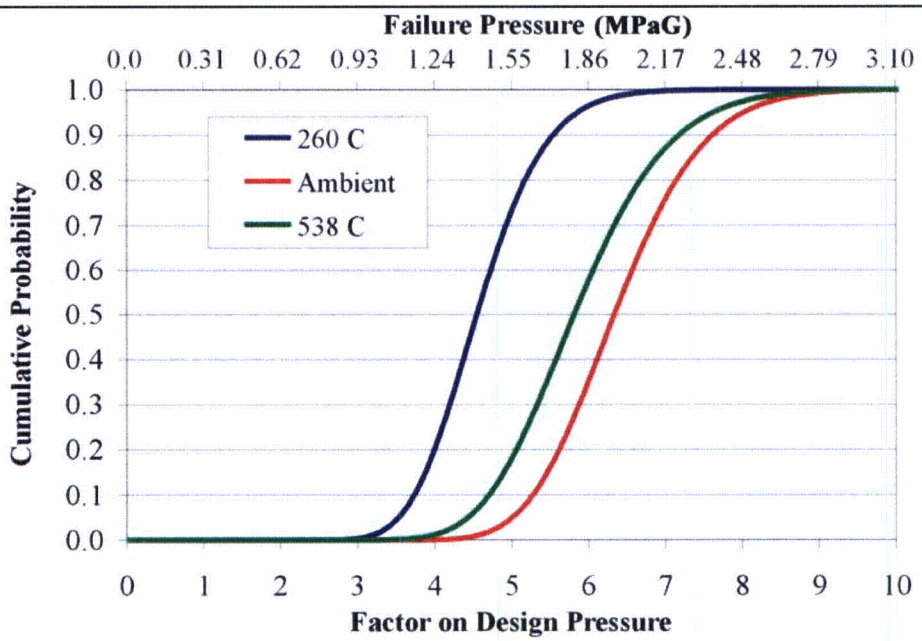

Figure 19C-11. Pressure Fragility with Temperature for Leakage at Drywell Head

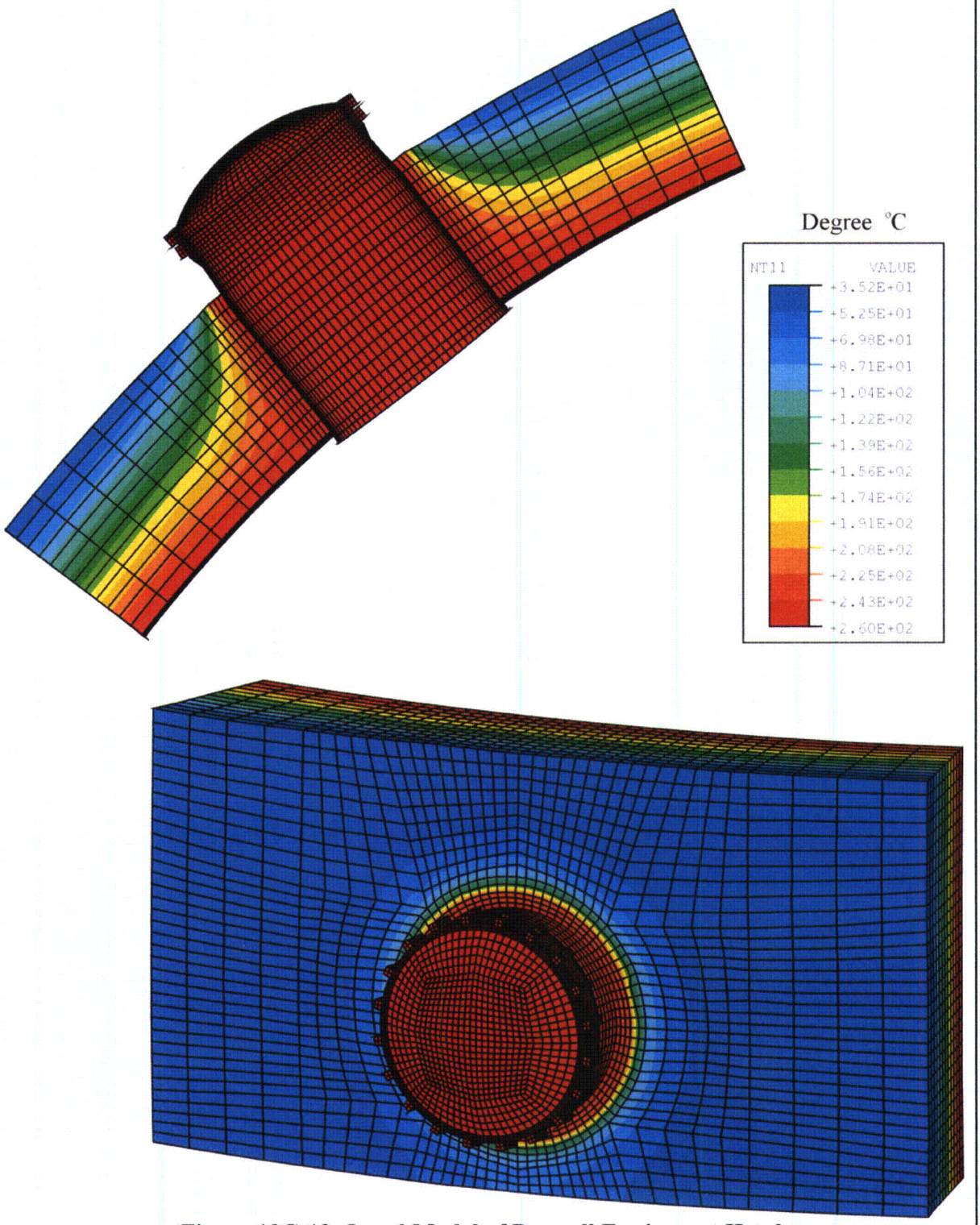

Figure 19C-12. Local Model of Drywell Equipment Hatch

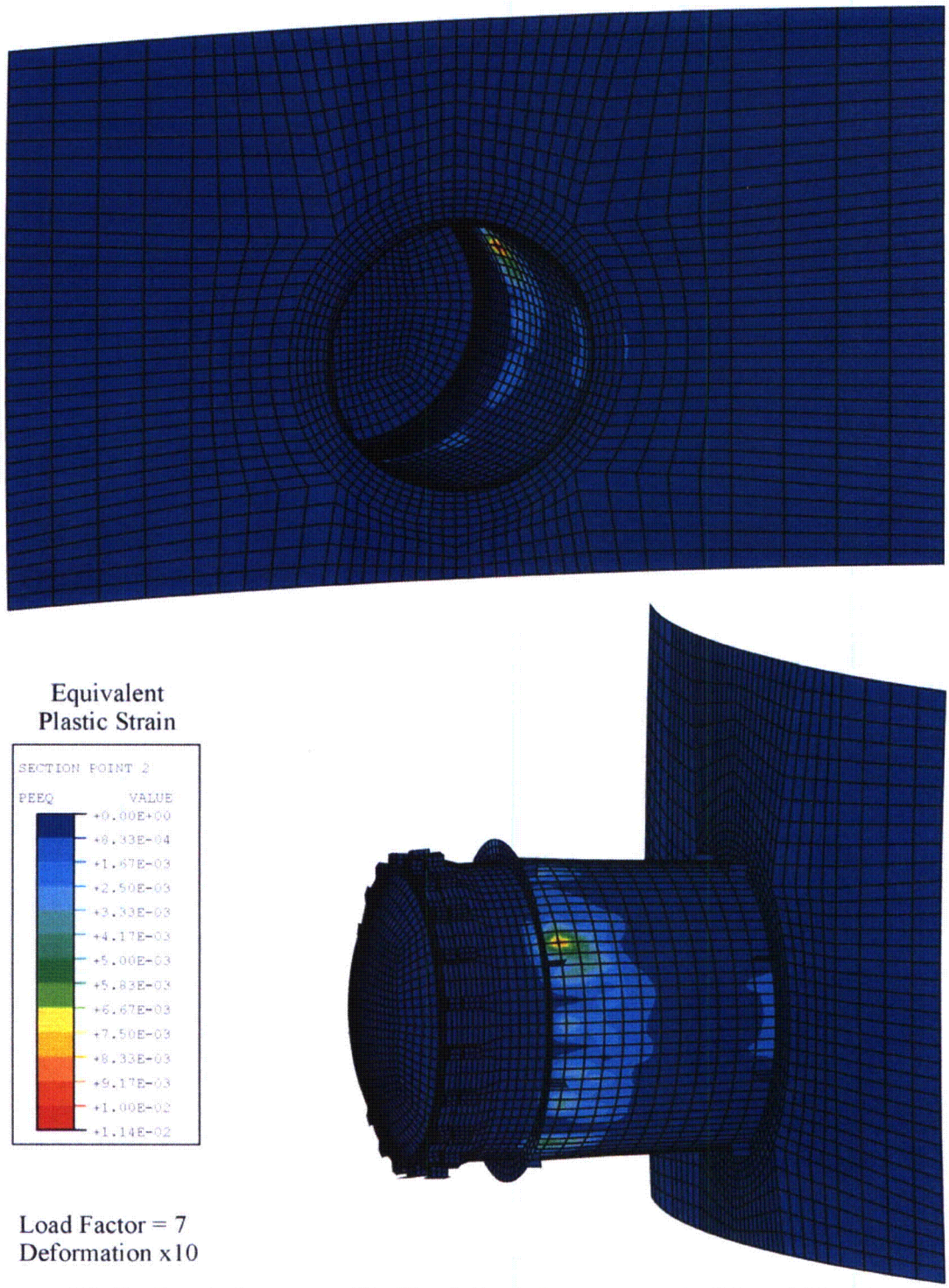

Figure 19C-13. Plastic Strains in EQ Hatch Steel Components, 260°C (500°F) Conditions

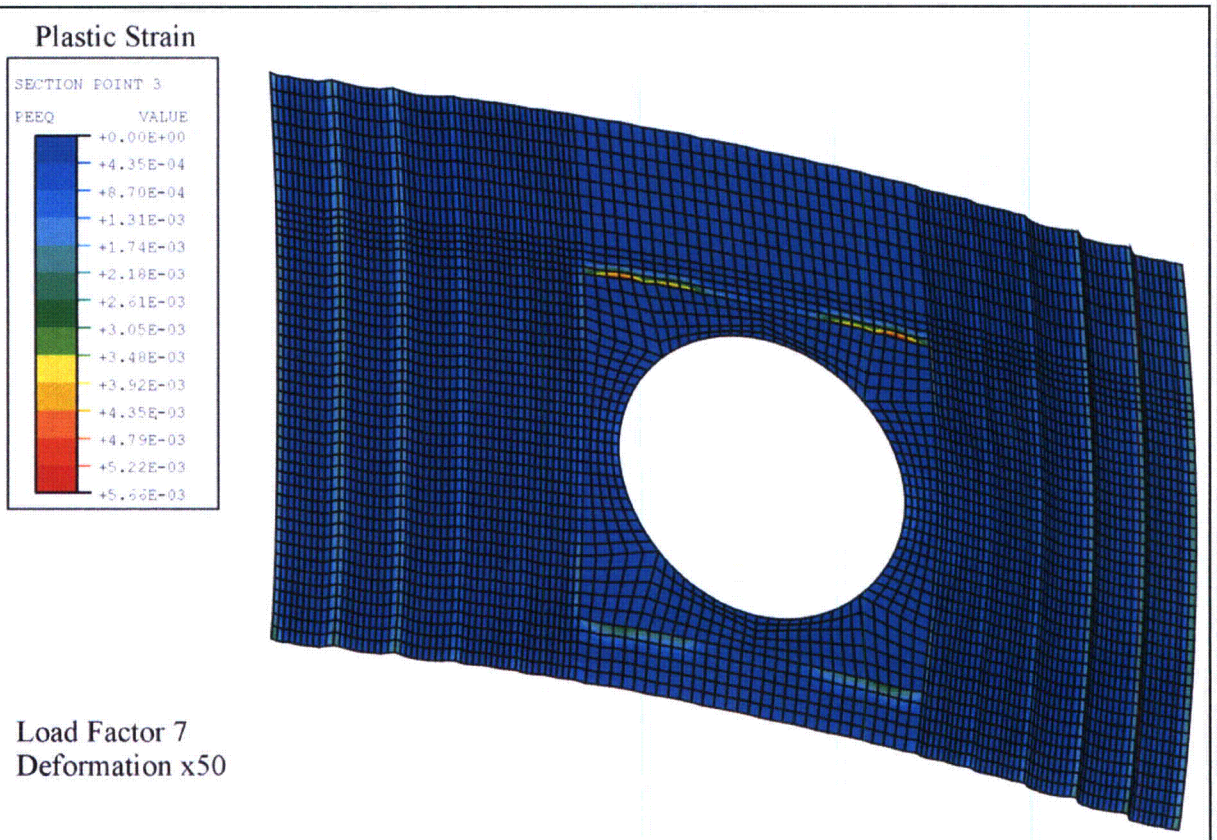

Figure 19C-14. Plastic Strains in Liner for Local Effects Slice Model

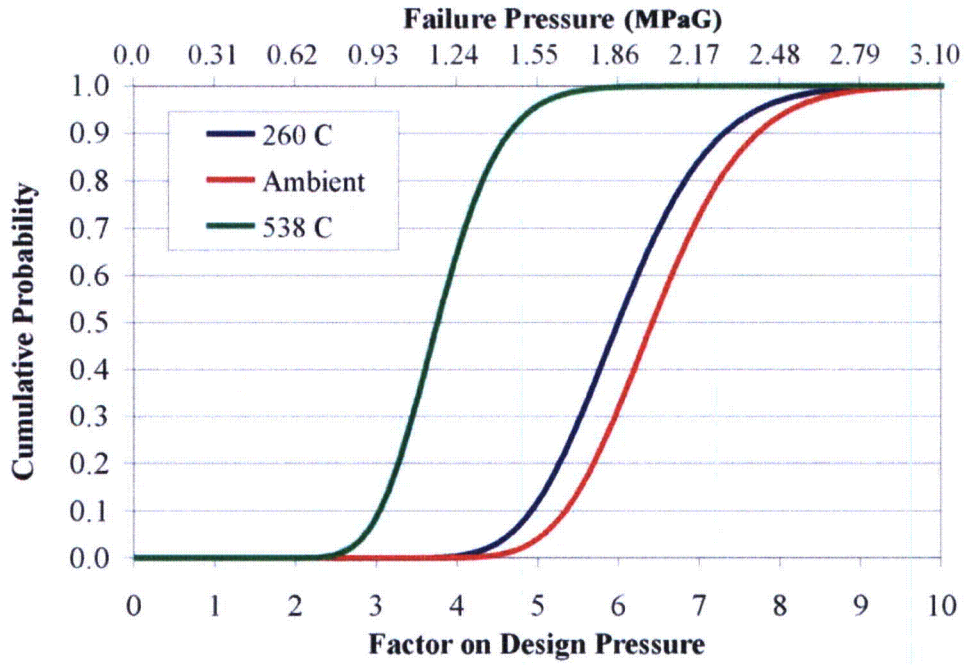

Figure 19C-15. Pressure Fragility with Temperature for Leakage at Equipment Hatch

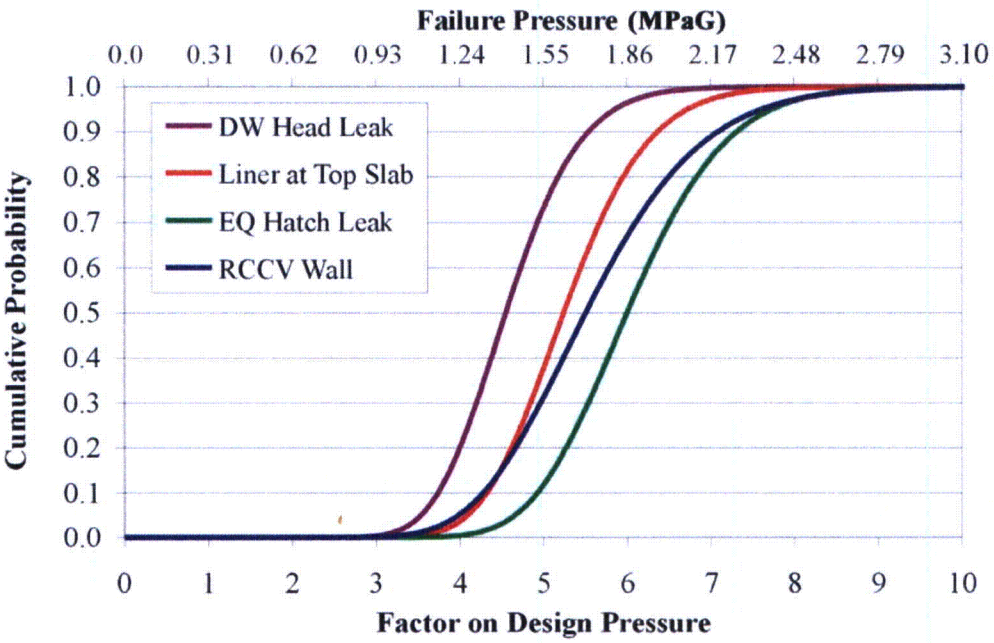

Figure 19C-16. Pressure Fragility at 260°C (500°F) Steady State Thermal Conditions

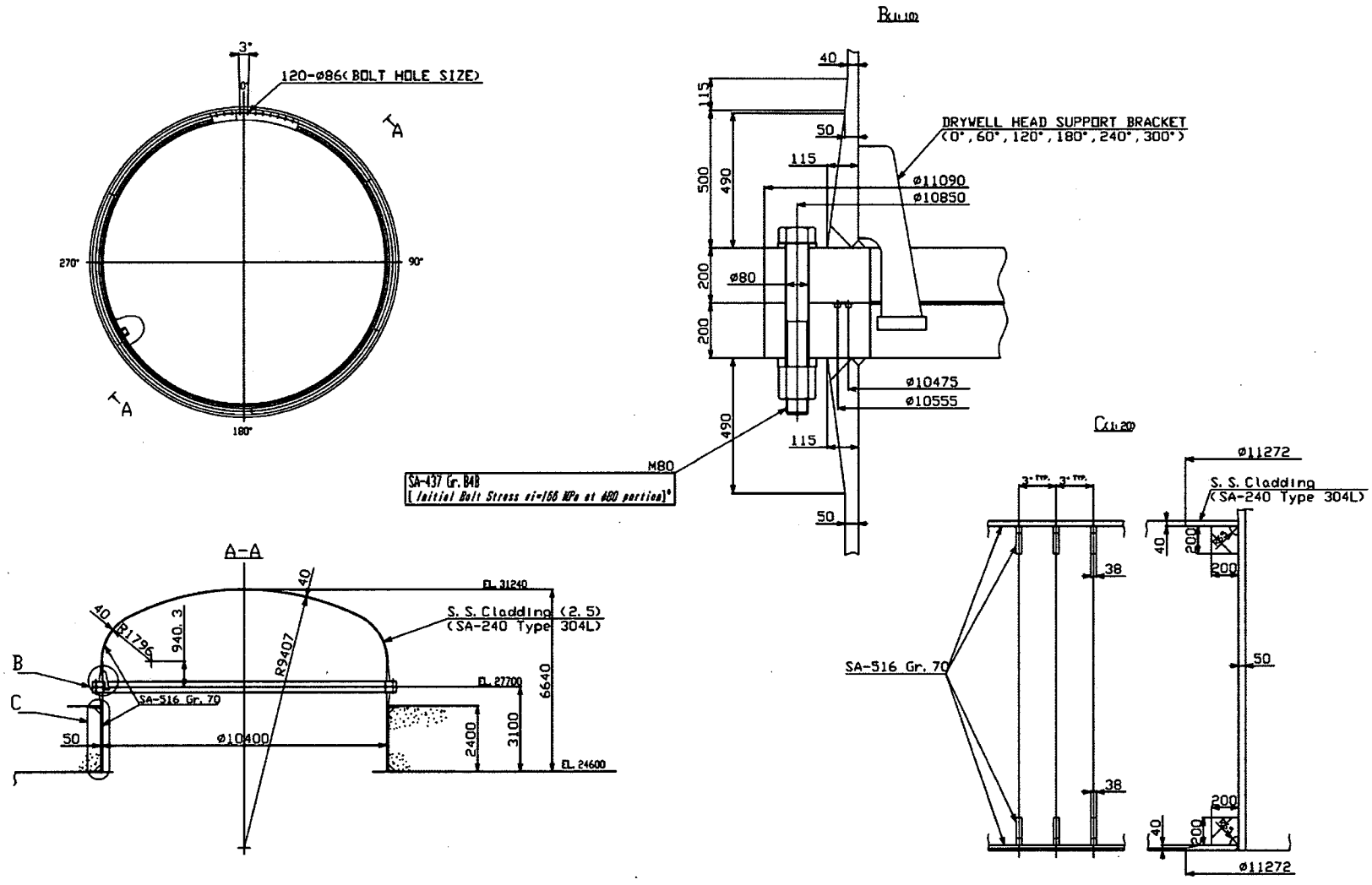

Figure 3G.1-51. Drywell Head

Enclosure 3

MFN 08-380

Figures 3G.1-52 and 3G.1-53

Non Security-Related

Figure 3G.1-52. Equipment Hatch

Figure 3G.1-53. Wetwell Hatch

{{{Security-Related Information - Withheld Under 10 CFR 2.390}}}